

FINAL REPORT

For

NASA Grant/Cooperative Agreement NAG-1-1933

Submitted by

**Joe Gray
Center for NDE
Iowa State University
Applied Sciences Complex
Ames, IA 50011**

Introduction

The final report of NASA funded activities at ISU for the period between 1/96 and 1/99 includes two main areas of activity. The first is the development and delivery of an x-ray simulation package suitable for evaluating the impact of parameters affects the inspectability of an assembly of parts. The second area was the development of images processing tools to remove reconstruction artifacts in x-ray laminagraphy images. The x-ray simulation portion of this work was done by J.Gray and the x-ray laminagraphy work was done by J. Basart. The report is divided into two sections covering the two activities respectively. In addition to this work reported the funding also covered NASA's membership in the NSF University/Industrial Cooperative Research Center.

PART 1

Overview of the Elements of XRSIM

The key elements that make up an x-ray radiography model include the x-ray source, a means to incorporate the part geometry, the x-ray interaction with the material, the detector response and, finally, a means to model the setup of the of the particular radiograph. X-ray tube sources have a wide range of properties including a range of kilovoltage, different inherent filtration, spot sizes and power loading. The radiation produced is a complex spectrum of white x-rays with a wide range of photon energy. Models of this spectrum require a means to handle electrons moving at velocities near the speed of light interacting with the complex of bound electrons in the target material. The model in XRSIM begins with the bremsstrahlung interaction cross sections for relativistic electrons and the bound electron in the target material (1). These cross sections are energy dependent and so the energy loss of the electron beam as it passes through the target material needs to be included. The white bremsstrahlung spectrum generated from this interaction is also attenuated by the amount of material in the target that the electron beam penetrates. In order to estimate this we use the target angle with respect to the electron beam and the electron penetration into materials to calculate the amount of target material that the bremsstrahlung spectrum must pass through in order to exit the vacuum window. The material and thickness of the vacuum window also contribute to the inherent filtration of the particular tube. The beam model assumes a thick target bremsstrahlung model – all of the electron kinetic energy is deposited into the target- with the exit port of the tube at 90 degrees with respect to the electron beam direction. The variables that can be controlled in the beam model are shown in Table 1 in the Appendix.

The interaction of x-ray photons with matter is highly non-linear and involves several processes competing for dominance. For elements with high atomic number, $Z > 40$, the low energy interaction is dominated by photoelectric absorption. The same x-ray spectrum interacting with a low atomic number material will produce much more scattering via Compton interactions. This behavior, of course, assumes comparable thickness of each material, with the implication that as the thickness of the high Z material increases, so too does the scattering. Absorption coefficients for alloys and compounds are easily determined using a rule of mixtures for the elemental constituents of the material and knowledge of the material density. The absorption coefficients used in XRSIM track the energy dependence of the total linear coefficient. The energy dependent absorption is computed using the linear attenuation coefficients. These data for each element are widely available from several databases.

The conversion of the transmitted x-ray beam into the image viewed on a film or in an image intensifier involves a multi-step conversion process. Most of the noise processes that dominate the image are a result of the detector characteristics. In film the grain noise, speed of different film, the use of several types of intensifying screens all must be modeled (2-6). In a real time system based on an image intensifier, noise includes the CCD camera pixel non-uniformity, the thermal noise in the CCD chip and the systematic artifacts introduced by the image intensifier tube. Finally, the response of a detector must be a function of the dose deposited into the detector; otherwise the detector response will depend strongly on the average energy of the transmitted x-ray beam, figure 1. This last point is a key issue. Most detector response curves are based on a particular spectrum. For example the H and D curves published by film manufacturers are valid for the kilovoltage selected, typically 250kVp, the filtration used and often for that particular x-ray tube. In a simulation of the image formation process, different thicknesses of the material will transmit different spectra. The result is a widely variable set of spectra hitting the detector at various points. By using the absorbed dose method of characterizing a detector, a universal response curve can be generated. In this model we use the fact that the detector response is measured as a function of the absorbed dose in the detector. This last point is also important. The aforementioned H and D curves are measured as a film response against exposure. This exposure is measured for air, as is typical of standard ionization gauges. This also introduces errors in that the quantum efficiency of an ionization gauge is quite different from other x-ray detectors.

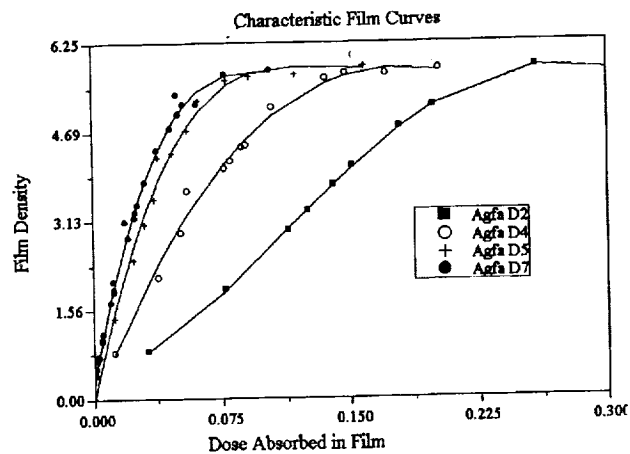


Figure 1 The response curve for a number of Agfa films. Data points on this curve are taken with different filtrations, different kilovoltage setting and through different types of part material. The result when using the absorbed dose approach is a universal response curve.

Last, but not least, the complexity of the part shape and of the flaw shape has a profound effect on the subsequent image, for example, the part geometry and its orientation can play a key role in understanding the image. Of course the defect morphology can have an equally critical impact, for example, tight fatigue cracks in complex part geometry are notoriously difficult to detect. An added difficulty in modeling this process is the need for sophisticated visualization tools, nature places the defect in a part at a particular location in a specific orientation. The modeling program must have the flexibility to allow precise placement, both location and orientation of computer representations of the part and defect.

As can be seen in figure 2, the radiography simulation program provides a full 3D visualization capability to allow the user to manipulate the part, arrange assemblies of several components and place realistic defects in any location. In the simulation of radiography we import the geometry from a CAD representation, specifically as a surface of triangular facets. All of the common CAD packages have a feature to produce this format including Catia, ProE, AutoCAD, Anvil, Unigraphics and I-DEAS. The complexity of the geometry of the part or the defect is limited by the capabilities of the CAD modeling environment or in some cases limits computer memory.

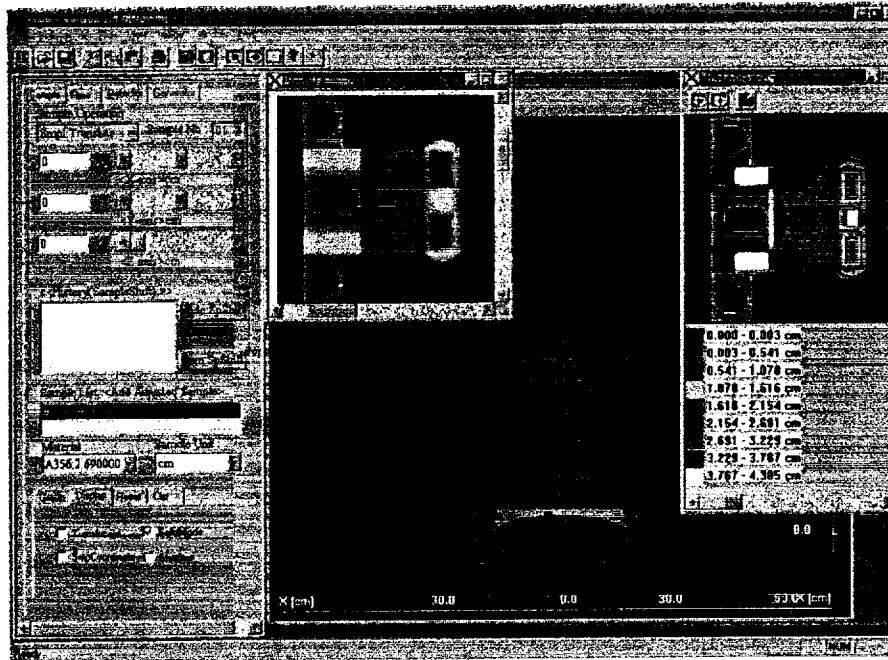


Figure 2 A screen shot of the graphical interface of XRSIM showing several parts with flaw placed in different locations. The central portion of the image shows the radiographic setup of the part in the x-ray beam. The image to the right is the resulting projection thickness for the selected part orientation. The defects are shown as the two large dots in the web region of the part. The image to the left is the simulated radiograph.

Examples of the types of images that are routinely produced using XRSIM are shown in figure 3. These parts are of moderate complexity and take less than a minute to calculate on a 200 MHz Pentium PC with 32 MEG of memory. The orientation of the part and positioning of the part can be set. The addition of defects, cracks, voids and inclusions complete the ability to determine defect detectability. The effects of different conditions used to generate the radiograph can be modeled. For example, the effect of filtration and the selection of the tube voltage control both the latitude of the radiograph and the contrast sensitivity. In effect at high tube voltage with filtration a larger range of part thickness can be covered in one radiograph, but at the expense of a loss in sensitivity.

An important part of any simulation is the experimental validation. The plots in figure 4 show the predicted density for a series of sample thickness plotted with the measured film density. The right hand plot shows the calculated and measured contrast between adjacent steps of the step wedge. As can be seen in these plots, the agreement between XRSIM and experimental data is good. A final point regarding the accuracy of the model should be made. As with any model that

balances computation time on reasonable computer platforms with the accuracy of the simulation, approximations are made. The results in figure 4 show results typical of the simulation when these approximations are reasonable. If the scattering intensity reaching the detector is of the same size as the transmitted flux, the simple scattering model in XRSIM will break down with an increasing discrepancy in the predicted film density (17-18).

Application of an X-ray simulation program

There are a number of applications to which an accurate x-ray inspection simulation capability can be applied. Some of these include determining optimal inspection parameters such as selection of the x-ray tube, type of film, and part setup. Once these initial issues are determined, the question of inspection coverage, limits of detectability and optimizing the performance of the inspection at reduced cost become key issues. An example of this type of optimization is the selection of the tube kilovoltage.

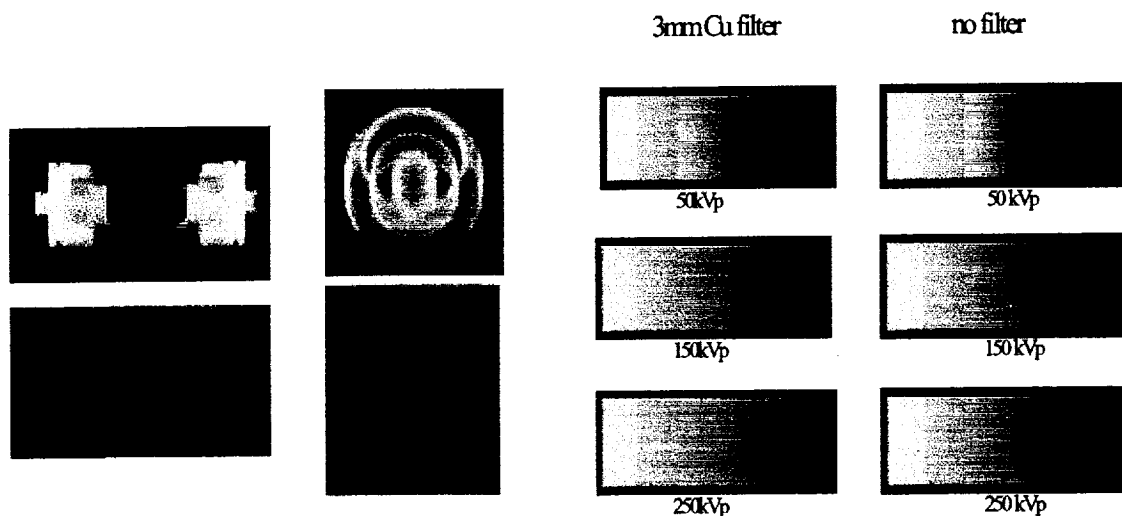


Figure 3 The image pairs to the left show CAD solid models and the corresponding simulated radiograph. These two parts illustrate relatively simple part geometry. The stepwedge images to the right show the effect of beam quality on the radiographs. The effect of the tube kilovoltage on latitude and contrast is illustrated. With the copper filter on the left, the latitude is noticeably greater even at the higher voltages. The effect on kilovoltage on contrast can also be seen.

Generally, the closer that the kilovoltage is set to the maximum of the tube the shorter the exposure times required to reach a desired film density. The effect of kilovoltage on latitude versus contrast is well known. In figure 3 we show the effect of kilovoltage and filtration on image quality.

By placing defects of different size in areas of interest in the part, we can rapidly determine the minimum detectable defect size for the setup and parameters selected. It

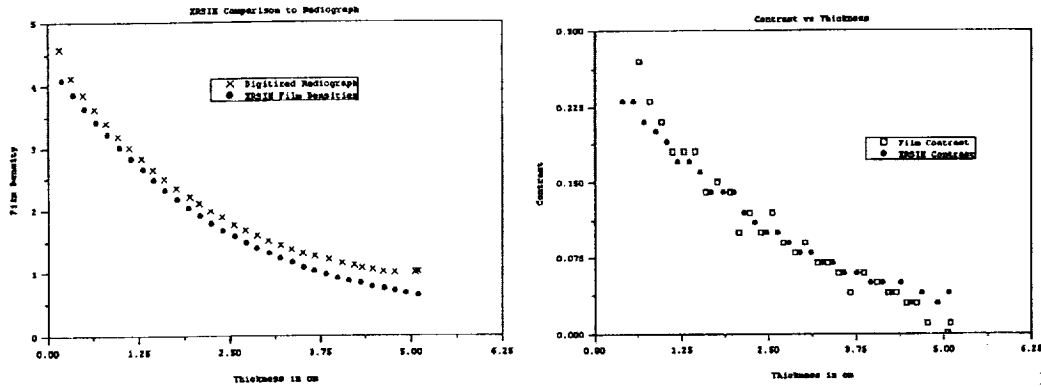


Figure 4 Two plots show results of the experimental validation of the model. The left plot is a comparison of the film density as predicted using XRSIM and as measured from a radiograph. The plot on the left shows the contrasts from the same image. In this plot the experimental results are indistinguishable from those from XRSIM. The data was taken from a film using 250 kVp generator setting, a 30 mil Cu filter on D7 film.

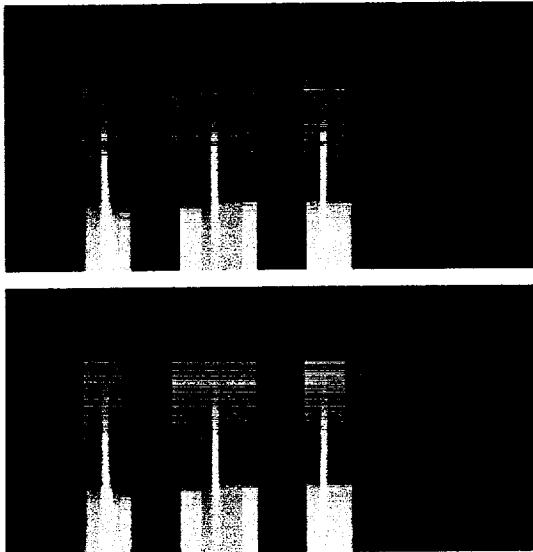


Figure 5 Flaw sizes ranging from 5mm to 0.125mm are shown. The larger flaws easily seen, while those below 0.25 mm are undetectable. These detectability limit were computed in a few minutes with XRSIM.

is quickly found the in addition to the beam quality that the limit of detectability varies as a function of sample thickness and exposure conditions. The power of a simulation capability is illustrated with this example, shown in figure 5. In the two radiographs the contrast from each of three defects ranging in sizes from 0.125 mm to 5 mm is shown. The large defect is easily seen, while the 0.125 s not detectable. One of the difficult elements of experimentally determining this type of result is collecting the requisite examples with an appropriate range of defects at the locations of interest, for example, the high, and stress regions of the part. The cost of assembling these samples quickly grows. Further, the part must be in a prototype stage to even begin the collection of images of different defects. A simulation capability with a limited set of real

samples for validation can greatly extend the range of variables examined. This study can be done at the early design stages where inspectability issues are rarely able to have impact.

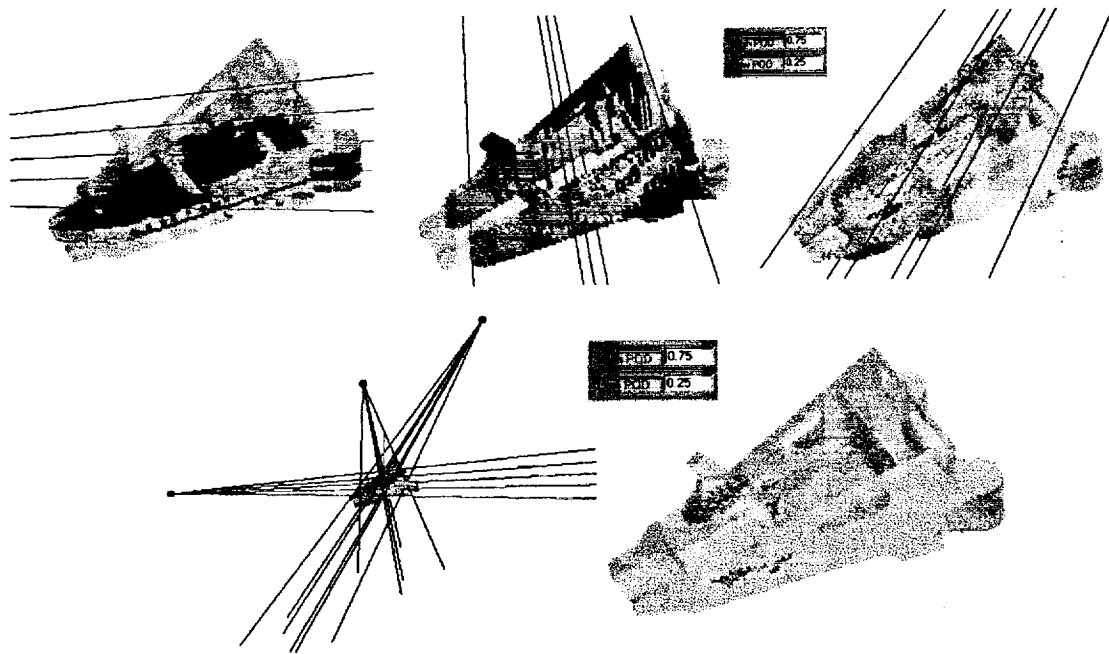


Figure 6 The top three images show the detectability for three specific inspection directions. The red areas show that the flaw placed at each of these locations in the part are undetectable, the transparent areas show inspectable regions. The yellow color represents regions of intermediate detectability. The lower two images show the inspected region obtained by combining the results of the three separate inspection directions.

The capability to determine the detectability of a critical defect by means of a particular inspection technique allows detectability maps to be computed, see figure 6. The detectability map shown is computed by dividing the CAD model into a grid and placing a defect at each grid location in the part. Locations with flaws that are easily detectable, as determined by a signal-to-noise measure, are made transparent. The locations that have undetectable defects are colored red and the intermediate flaw sizes are yellow. These maps very rapidly show the coverage of a particular inspection plan for the part. This example of inspection coverage shows only the effect of part orientation. As indicated earlier, the beam quality also has a strong influence on detectability. This tool to visualize the inspection coverage provides a means to determine optimal inspection conditions at a minimum cost (19).

Study Using XRSIM to Detect Explosive Separation from the Casing

One of the studies requested by NASA was to use XRSIM to examine the detectability of a gap forming between the explosive and the metal casing of an artillery shell. The issue in this case is that a gap causes the shell to explode in an unpredictable manner. There are two key parameters that need to be examined, the size of the disbond and the gap between the disbond and the shell casing.

The first step was to develop a CAD solid model of the shell geometry, the explosive and the delamination. Based on drawings supplied by NASA, the CAD models shown in figure 7 were developed. The solid model used to represent the geometry of the part can be refined in the CAD model to present a smooth surface with considerable detail. In figure 8 the model for the explosive filler for the shell casing together with the model for a shell casing is shown.

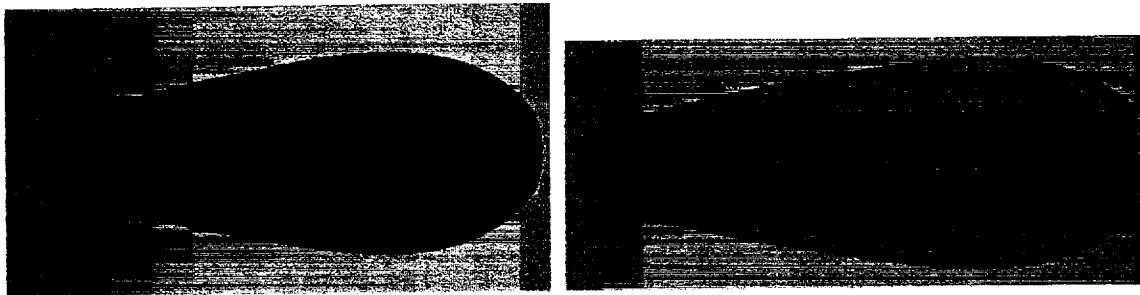


Figure 7 A CAD solid model of the shell casing developed for explosive delamination studies. The image on the left is the solid model view of the triangular faceted surfaces shown on the right.

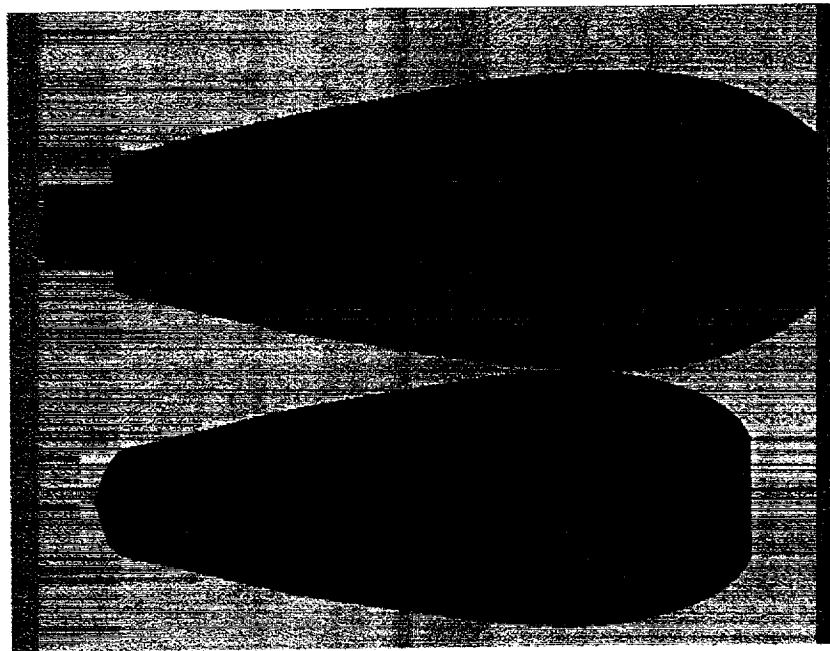


Figure 8 The CAD model for the explosive that fills the shell casing is shown. The explosive is the lower object. On the right is the assembled shell.

The assembly of several parts into a single unit can be accomplished in two ways. The first is to prepare the components in the CAD development package registering the repetitive positions of the elements of the assembly. The second way is to import each component into XRSIM. The registry of the components can be done by using the translucent feature of the display.

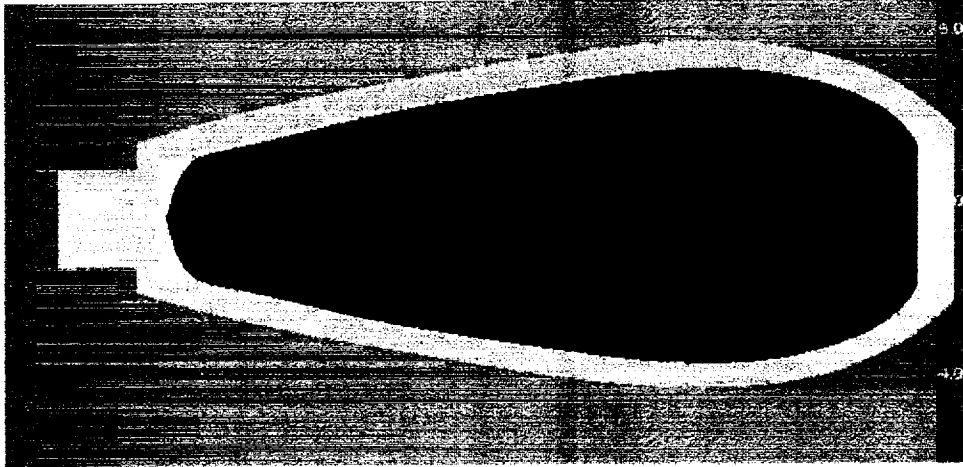


Figure 9 The explosive core has been placed in the metal shell. A slight miss alignment can be seen at the left end. The thin white region is where the explosive has not been placed properly in the CAD model of the shell.

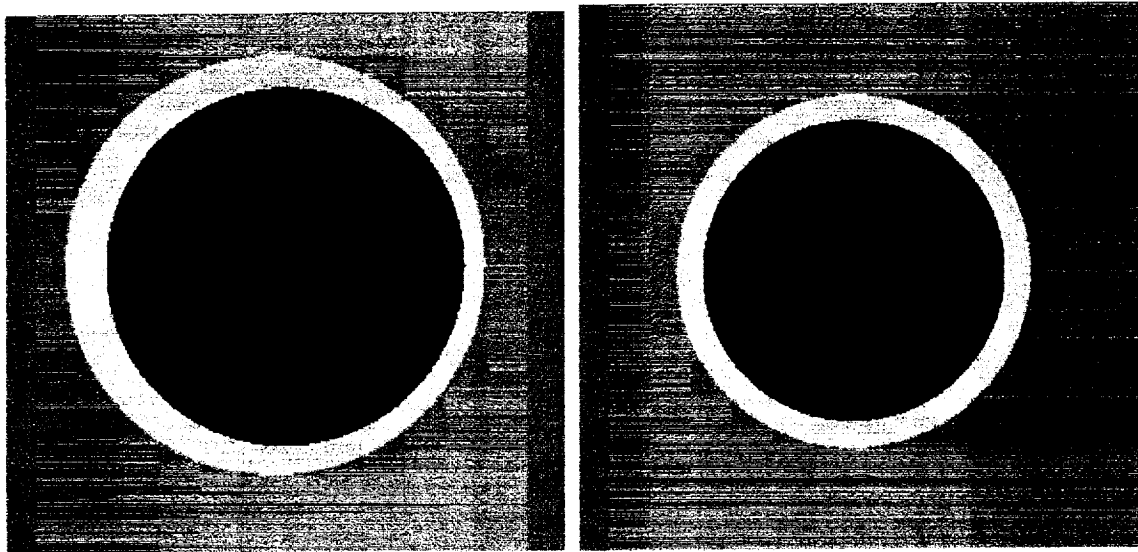


Figure 10. Viewing the assembly on end as seen on the left shows a slight misalignment. The image on the right shows good alignment of the two CAD objects.

The final step in the process is to place the flaw at the appropriate location. Figure 11 shows such a placement.

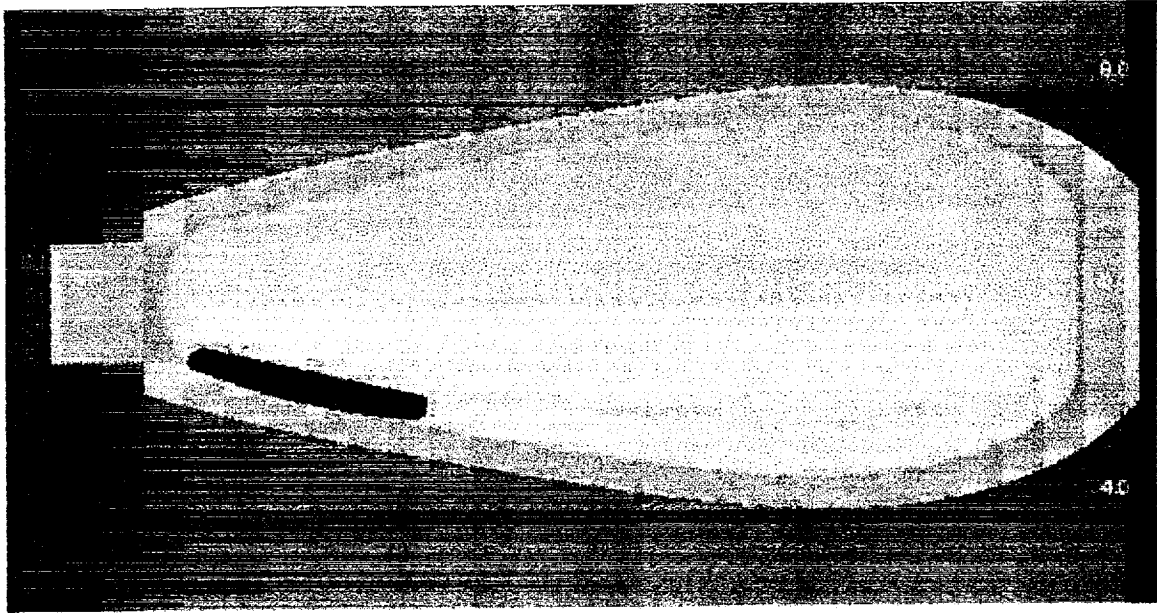


Figure 11 The final assembly of the CAD objects, the artillery shell casing (bright yellow), the explosive(light yellow) and the delamination(green).

The size and location of the delamination can be controlled by scaling the CAD model for the flaw. The opening of the delamination can be varied by scaling the z-direction of the flaw. The orientation of the delamination with respect to the x-ray beam is controlled by rotation the CAD models for the shell casing and the explosive. This is accomplished by using the group feature in XSRIM. By grouping the casing and explosive, any translation or rotation applied is applied to the whole unit. One to four flaws may be added to each CAD object. This allows the user to place several delaminations in the different locations.

There are several additional parameters that must be specified in order to complete the part description. The material of each component must be selected. The alloy used in for the casing is 304 stainless steel and the explosive material is TNT. The addition of new materials, for example different explosives, can be done by specifying the atomic weight percentage of the elements making up the compound or alloy. XRSIM has with the distribution the elemental absorption coefficients for all the elements with $Z=1$ through $Z=94$.

The effect of the opening between the shell casing and the explosive is illustrated in figure 12. The images in figure 13 show the result of rotating the casing so that the delamination is aligned with the x-ray beam, at 15 degrees to the beam. Although the delamination is wide, only in the aligned orientation can the delamination be seen. This illustrates the sensitivity to orientation that the detectability of a crack has as a function of the orientation. From the orientation data shown in figure 13, we can estimate the number of orientations needed to provide full coverage. The rotation angle is dependent on the size of the gap, specifically as the gap becomes narrower, smaller changes in orientation for the next view are required.

The point illustrated in this example is that XRSIM provides a powerful tool to develop inspection specifications in a quantitative fashion. The ability to simulate the effect of different parameters such as kilovoltage, part orientation, flaw and parameters is difficult to duplicate in an experimental setting. The likelihood of finding a satisfactory range of flaw parameters in actual components is unlikely. The cost of fabricating the same set of artificial flaws is costly.

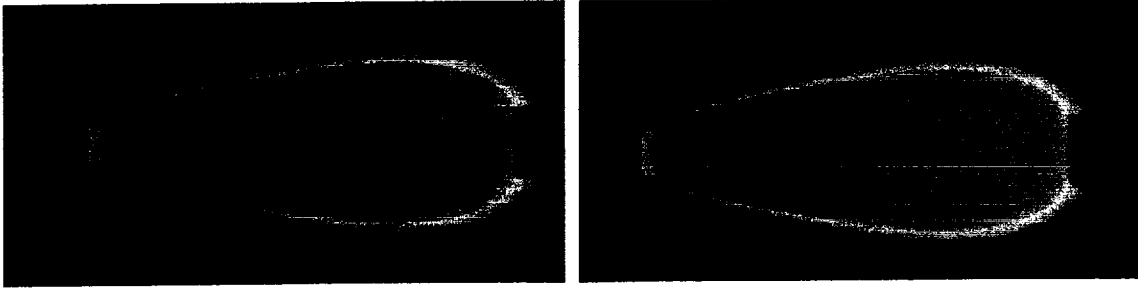


Figure 12 The left image shoes a delamination between the shell casing and the explosive. The gap is 0.3 mm. The image on the right is for an opening between the explosive and the case of 0.1 mm.

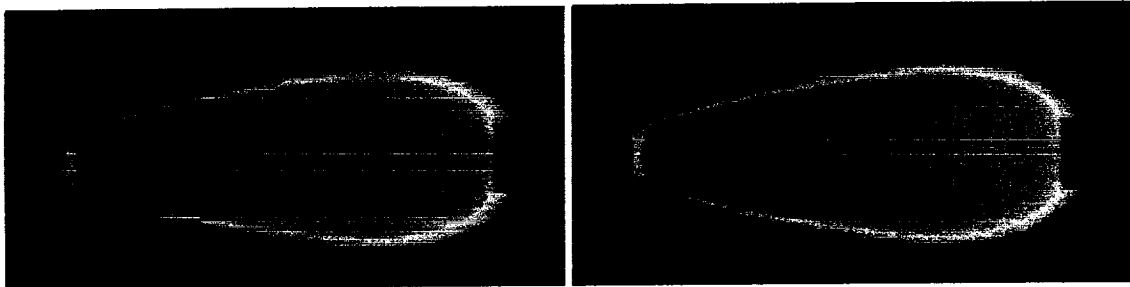


Figure 13 The delamination easily seen in the left image becomes very difficult to identify in the right. The shell was rotated around the axis of the shell by 15 degrees.

Further the time needed to generate the actual images is much larger than the time to generate the simulated results. Indeed a typical image from XRSIM takes several minutes to obtain from an initial setup. This is compared to the 8-10 minutes required for just the film developing.

Summary of Activities

The principle focus of the work done in this portion of the activity was the support and development of the x-ray simulation program. This work was beyond normal activity which was part of the Center for NDE membership. Some of the activities done include custom development of XRSIM for a Sun Unix platform, later delivery of a Windows PC platform version, modeling extensions including multiple flaw capability, added file formats, multiple objects, crosshair for showing flaw location, CAD object registration, Cad placement by absolute coordinate, various bug fixes and reverse geometry tube spectrum, thick filter effects. A program for calculating x-ray absorption coefficients for user specified alloys and compounds were supplied. A user manual, included with this report was supplied. Finally, initial development of a first principles x-ray scattering model was begun.

References

1. C.M. Lee, L. Kissel and R.H. Pratt, (1976) ' Electron Bremsstrahlung Spectrum'', Phys Rev A Vol 13, #5, p1714-1727
2. J. Gray, , T. Gray, N. Nakagawa, R. B. Thompson, " Models for Predicting NDE Reliability," Metals Handbook, Vol. 17, 9th ed., ASM International, Materials Park (1989).
3. J. Gray, , "Three Dimensional Modeling of Projection X-Ray Radiography," Review of Progress in Quantitative Nondestructive Evaluation, Vol. 7A, ed. by D. O. Thompson and D. E. Chimenti, Plenum Publishing Co., 1988, p.343-348.
4. "A Model of X-ray Film Response" by Jensen, Aljundi, Gray, and Wallingford, "Review of Progress in Quantitative Nondestructive Evaluation", Vol. 15A, pages 441-448; Eds D. Thompson and D Chimenti, Plenum Press, New York, 1996
5. "Calculation and Measurement of Exposure Buildup Factors for X-ray Radiography" , T.Aljundi and J.Gray, "Review of Progress in Quantitative Nondestructive Evaluation", vol. 14A, p 339, Eds. D. Thompson and D Chimenti, Plenum Press, New York, 1995
6. F.Inanc and J. Gray, Applied Radiation and Isotopes, vol48, #10-12, p 1299-1305 (1998)

Part 2

Laminography

Introduction

The research work on laminography was done in two projects, each one of which was associated with a graduate student. The first project was associated with planar geometry. During this project we became familiar with laminography, its geometry, and associated problems. We completed a first attempt at removing artifacts in laminographs. The second project was more ambitious and undertook the task of removing artifacts from nonplanar objects. Both projects were successful within the scope of their objectives. For published papers see Hsieh and Basart (1999), and Hayee and Basart (2000).

Project No. 1: Artifact Removal from Planar Objects.

This project constituted the MS research of Hanyi Hsieh (1999). It started with the analysis of radiographs of a simple grid. There were eight independent radiographs corresponding to eight detectors in the reverse geometry x-ray system used to make the radiographs. When a laminograph was made using the group of radiograph, the result was as shown in Figure 1.

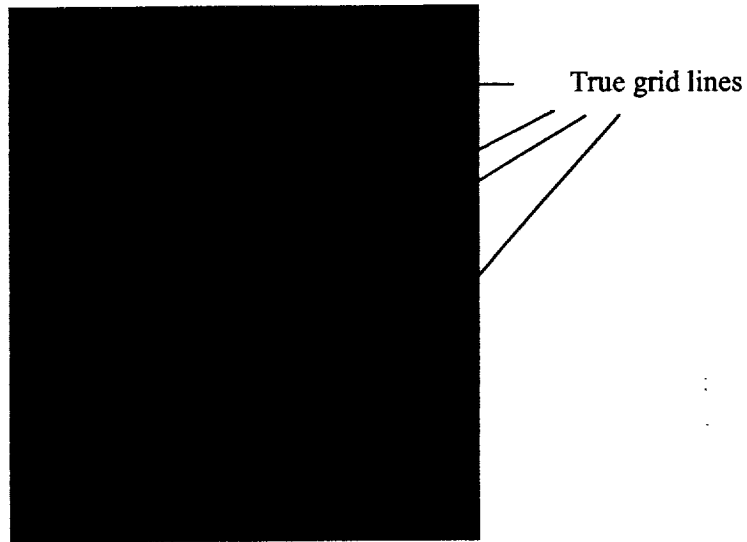


Figure 1. Laminograph of grid structure. True grid lines are indicated. The remaining structures are artifacts.

The object of our research was to invent a method for removing the artifacts (non-real grid lines). Even with a structure as simple as this, there were a number of signal processing. These consisted of alignment of the radiographs, low-pass filtering to reduce the noise in the image so that noise would not be falsely interpreted as a desired feature. Of course, this filtering blurred the desired features, but this was corrected in subsequent processing steps.

The next step was edge detecting and thresholding. Thresholding produces a binary image as shown in Figure 2. The grid lines are clearly emphasized, but so are many spots of noise. The next step of detecting edges eliminated most of the noise because the noise does not fall in the pattern of an edge. The grid lines appear as double lines because of the finite width of the lines and edges were detected on each edge of the line. Binary images were made of all eight radiographs.

Feature extraction was the next step. This process is very powerful for reducing noise. Cross correlations were made between various pairs of binary images. The pairs of images giving the highest cross correlation were used for further analysis. It was assumed that large correlations were indications of true structure, and all other stuff in the image could be ignored because it was false structure.

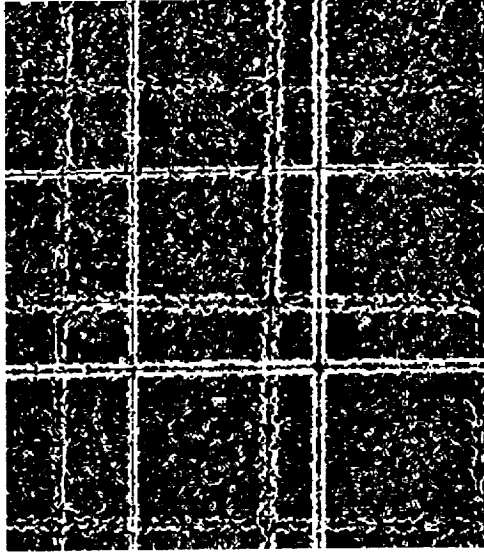


Figure 2. A binary image made by features thresholding and edge detecting a gray-scale image.

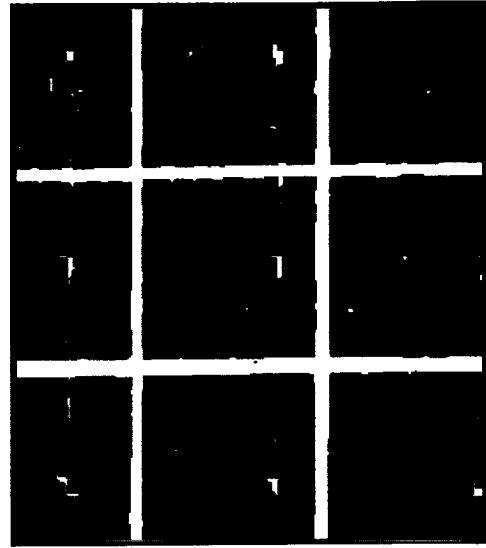


Figure 3. Binary image after are extracted and processed with dilation and erosion.

The assumed true structure was extracted and put into a new image. This structure was far from usable in this form because of the double edges and discontinuities along the edges. To fill out the edges and merge each pair of double edges into one line, operations of dilation and erosion were used. Dilation blurred things together creating solid lines and joining broken line segments. It also widened the lines. To reduce the line width back to its correct value an erosion operation was performed. This is not an inverse dilation operation because these operations are nonlinear. That is, when line segments are joined together by dilation, erosion does not pull them back apart. The results of the processing of one radiograph at this stage are shown in Figure 3. There are still a few unwanted features in the image, but the line structure is vastly improved. At this point in the processing the computer has automatically identified the desired structures.

The next step is to make intensity corrections in the images. The path length from the x-ray source to the sample and on to the detector varies for various points in the sample. Since the intensity in the far field of a source drops off as the inverse of distance squared, the intensity across an image was corrected by scaling the intensities by distance squared. The distance dependence was determined from a smoothed plot of intensity versus position for each slice through the image. Raw and smoothed slices of intensity along the 100th row in the image in Figure 1 is shown in Figure 4. The plot is smoothed to minimize the effects of "transient" structure in the image making the distance dependence more obvious. By least squares fitting a parabola to the smooth curve, we get a function that is used to correct the intensities for distance dependence. This is done for each row in each of the eight radiographs.

The final step is making a laminograph for a particular plane through the physical sample (the object being radiographed). The equations of the geometry are applied so the computer can eliminate artifacts.

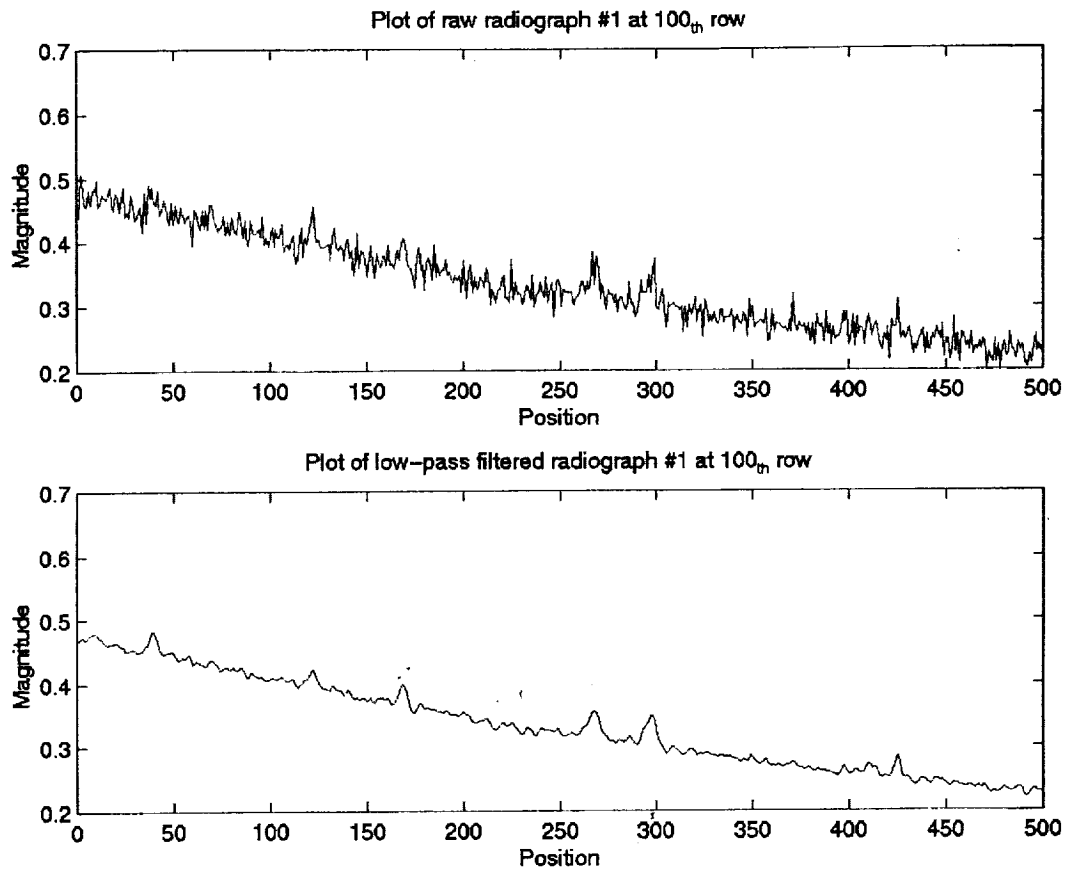


Figure 4. Unsmoothed (top) and smoothed (bottom) slices of intensity versus position along the 100th row of the image.

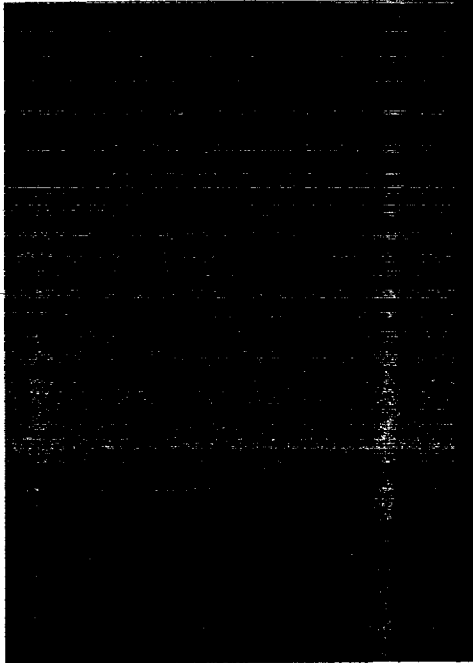


Figure 5. Final radiograph made after numerous steps of image processing.

The eight clean binary images contain the information for distinguishing between wanted and unwanted structure. The resulting laminograph is shown in Figure 5. Comparing Figure 5 with Figure 1 we can clearly note the improvement made by the processing. For further details on this entire procedure, see the MS thesis by Hsieh (1999).

Project 2: Artifact Reduction for Objects with Complex Geometry.

Sobia Hayee completed her MS research (Hayee 2000) creating a computer procedure for reducing artifacts in complex objects. She started with an ancillary project of studying the rather new procedure (at that time) of applying a differential equation to an image. This intriguing procedure is based on introducing the concept of time into image processing. This is accomplished by considering each stage of processing as a time step. Its main application has been to edge detection. It can produce a superior result at the expense of a considerable amount of processing time. Recall that edge detection was an important step in project No. 1. Although this differential equation process was not used for artifact reduction in Project 2, we briefly review it because it will likely be more prominent as faster computers are developed. For more details see Hayee (2000).

Anisotropic diffusion edge detection.

One way to deal with the problem of noise in edge detection is by image smoothing. Smoothing can be done by convolving the original image with a Gaussian kernel. The original image can then be represented by a set of derived images obtained by convolving the original image with a Gaussian kernel of increasing variance. Each of these derived images corresponds to the original image at coarser scales. Suppose $I_o(x, y)$ is the original image convolved with a Gaussian kernel $G(x, y; t)$ of variance t ; the resulting image obtained is

$$I(x, y, t) = I_0(x, y) * G(x, y; t) \quad (1)$$

Larger values of t correspond to images at coarser resolutions as is shown in Figure 6. This figure shows an original image and its smoothed versions. The original image is at the bottom and as we move towards the top, smoothed versions of the original image are shown at each step with increasing variance of the Gaussian filter.

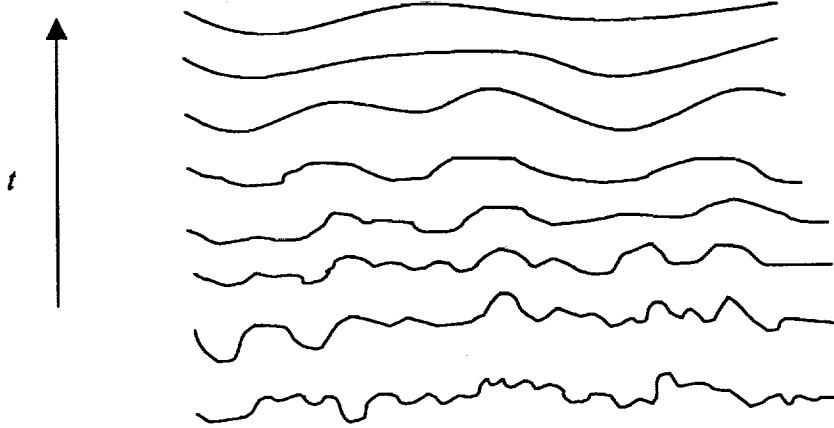


Figure 6. A set of derived 1-D signals obtained by convolving original signal (bottom) with Gaussian Kernels whose variance increases from bottom to top.

This figure can also be considered as a representation of conduction with t as the time. Hence we say that t is a pseudovisible. Such a set of derived images can also be viewed as the solution of the heat conduction equation or the diffusion equation. That is,

$$I_t = c\Delta I = c(I_{xx} + I_{yy}) \quad (2)$$

where $I_t = \frac{\partial I}{\partial t}$, $I_{xx} = \frac{\partial^2 I}{\partial x^2}$, $I_{yy} = \frac{\partial^2 I}{\partial y^2}$ and c is the diffusion coefficient.

The initial condition for equation (2) is that at $t = 0$; $I(x, y) = I_0(x, y)$, where $I_0(x, y)$ is the original image. The time " t " is a scale parameter; increasing t leads to simpler image representations. The embedding of an image into such a one-parameter family of simplified images is called scale-space.

In the multiscale or scale-space representation of an image it is impossible to find the true location of a boundary at the coarse scale image. The only way to obtain the true location of the edges that have been detected at a coarser scale is by tracking across the scale space to their position in the original image, which is a very complicated and computationally expensive technique. The reason for the loss of edge information is because Gaussian blurring does not preserve the natural boundaries of objects. To give a meaningful description of images at multiple scales the following criteria must be satisfied.

1. "*Causality*: No extra detail should be generated in the scale-space representation when passing from finer to coarser scales".
2. "*Immediate Localization*: The region boundaries should be sharp at each resolution and they should coincide with the semantically meaningful boundaries at that resolution."
3. "*Piecewise Smoothing*: At all scales, intraregion smoothing should occur over interregion smoothing."

When we look at the diffusion equation framework of the linear scale-space paradigm, we can see that equation (2) does not satisfy the three criteria stated above. To meet these objectives some modification in equation (2) is in order. So far the diffusion coefficient or conduction coefficient c is assumed to be a constant independent of the space location. There is no reason why it should be so. A suitable choice of c can satisfy all the three criteria stated above. Consider the anisotropic diffusion equation

$$I_t = \text{div}(c(x, y, t)\nabla I) = c(x, y, t)\Delta I + \nabla c \cdot \nabla I. \quad (3)$$

In equation (3), div indicates the divergence operator, ∇ and Δ represent the gradient and Laplacian operators, respectively, with respect to the space variables, and t is the time (scale). Equation (3) reduces to equation (2), the isotropic heat diffusion equation, if $c(x, y, t)$ is a constant. We want to choose a value of c that encourages smoothing within a region in preference to smoothing across the boundaries. This goal can be achieved by setting the diffusion coefficient to be "one" in the interior of a region, and "zero" across the boundaries. The diffusion will take place within a region and there will be no diffusion across the boundaries, as a result the region boundaries will remain sharp.

The problem is that the region boundaries at each scale are not known. At best an estimate of the location of boundaries can be computed. Suppose $\mathbf{E}(x, y, t)$ is such an estimate. Ideally this estimate should have two properties:

- (i) $\mathbf{E}(x, y, t) = 0$ in the interior of each region.
- (ii) $\mathbf{E}(x, y, t) = K\mathbf{e}(x, y, t)$ at each edge point, where \mathbf{e} is a unit vector normal to the edge at that point and K is the local contrast at that point.

If an estimate $\mathbf{E}(x, y, t)$ is available then the conduction constant c can be chosen to be a function $c = g(\|\mathbf{E}\|)$ of the magnitude of \mathbf{E} . The function $g(\cdot)$ has to be a nonnegative monotonically decreasing function with $g(0) = 1$. This way the diffusion will take place in the interior of the region and will not affect the region boundaries where the magnitude of \mathbf{E} is large. The level to which nonlinear diffusion equation is successful in satisfying the three scale-space criteria previously defined, depends on the degree of accuracy in estimating \mathbf{E} . Fortunately, the gradient of the brightness function gives an excellent estimate, i.e. $\mathbf{E}(x, y, t) = \nabla I(x, y, t)$. Hence, choosing the diffusion coefficient c as a function of the gradient magnitude of the image satisfies the scale-space criteria.

Given the mathematical framework described above, the next step mathematically is to develop a method for its implementation. The numerical schemes divide into implicit methods and explicit methods. The advantage of the explicit method over the implicit

method is that it creates a discrete scale space and there are no restrictions on the time step-size for the sake of stability. We will not go into further detail of this method here, please see Hayee(2000) for additional theory.

The results from this method are quite impressive. Figure 7 shows two simulated noisy images. The image sizes are 50 pixels by 50 pixels with white Gaussian noise (gray scale) introduced to a binary image of a white disk against a black background.



Figure 7. Simulated noisy images. The left image has a signal-to-noise ratio of 2.5 dB and the right image has an SNR of 5.0 dB

Figure 8 shows the edge images of Figure 7 obtained by a common gradient magnitude method. We see that the noise specks show up as edges especially in the left image in Figure 8, which is the noisier image.

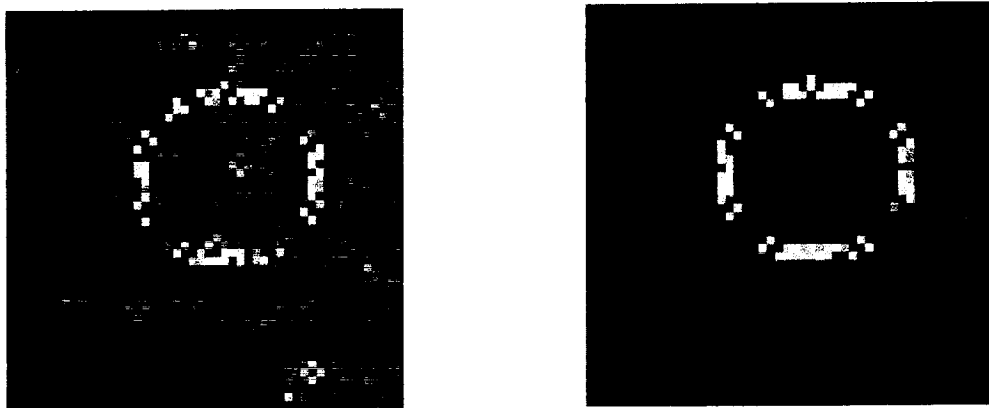


Figure 8. Edge detection by common gradient method.

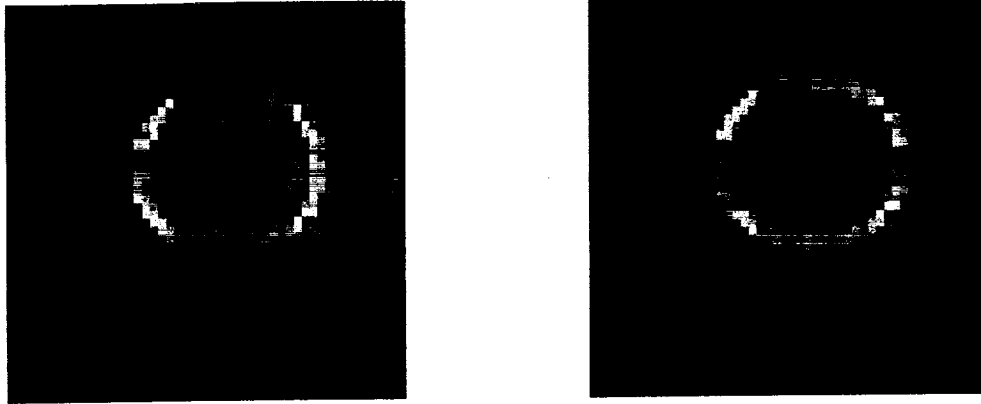


Figure 9. Application of nonlinear diffusion equation.

The results of this analysis were encouraging, but there was one huge drawback. The semi-implicit scheme is computationally very intensive requiring a lot of time for a single iteration. For a Pentium II 450 MHz Windows NT workstation, the time required for a single iteration of the nonlinear diffusion scheme on an image size of 50 x 50 pixels was approximately 28 minutes. The reason is simple. For an image of size 50 x 50 pixels we have a vector of size 2500 x 1 after vectorization of the image. Now the system matrix is of the size 2500 by 2500. It means that for an image of size M X N we shall have a system matrix of size MN x MN. The industrial images that we have are quite large in size. The image size of the digital radiographs used in this laminography project is 1000 x 1000 pixels. We can see that the size of the system matrix will be huge. The number of iterations will also have to be larger because real images have a lot of noise. Also the total number of radiographs is eight. So when we look at the time for a single iteration multiplied by the total number iterations required multiplied by the number of images, we end up with a processing time that is totally unacceptable.

Canny edge detection.

After investigating other various edge detectors, we settled upon another relatively new method, the Canny edge detector ((Canny, 1986).

Canny specified three criteria:

1. *Good detection*: The probability of failing to detect real edge points and falsely marking nonedge points should be low. This criterion corresponds to maximizing signal-to-noise ratio.
2. *Good localization*: The points marked as edges should be as close as possible to the center of the true edge
3. *One response to a single edge*: There should be only one response to a single edge, if there are two responses one of them should be considered false.

The Canny edge detection scheme describes a computational approach to edge detection. A mathematical form for the three performance criteria given above is developed which

can be used to design a filter which gives the best performance with respect to these criteria. Canny found that a kind of uncertainty principle applies when considering location and detection problems. A limit is reached beyond which improved detectability can be achieved only at the expense of poor localization and vice versa. A comparison, however, can be reached and a detector can be evolved. The derivation of the operator is mathematically very complicated. Fortunately we only have to use the result. For details of the application of the Canny detector see Hayee (2000).

Figure 10 shows the application of the adaptive Wiener filtering followed by the Canny Edge detector on the simulated noisy image shown in the left image of Figure 7. The results are very good and both the adaptive Wiener filtering and the Canny edge detection can be applied by only a single command in MATLAB. The reason that the Canny edge detector gives such good results is because it calculates both the strong edges and the weak edges, and the weak edges are included in the final edge map if they are connected to the strong edges. In this way this detector is more immune to noise. Adaptive filtering followed by the Canny edge detector is the noise reduction and edge detector scheme that we have used for our research.

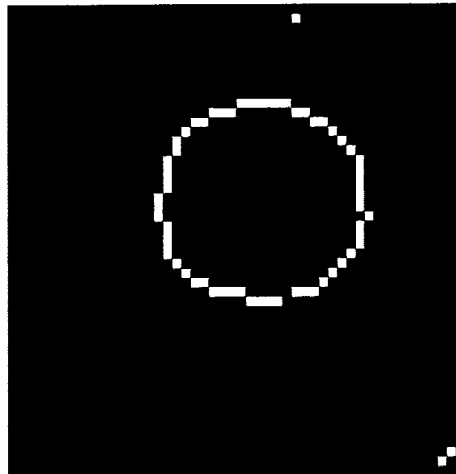


Figure 10. Image smoothing and edge detection by adaptive filtering followed by the Canny edge detector.

Cropping and enhancement

When dealing with objects with complex geometric structures, artifact reduction comes before the alignment of radiographs to make a laminograph. At first this method seems to be nothing like an artifact reduction method. The first question that comes to mind is how can you identify artifacts before making a laminograph? Artifacts are the shadows that appear in a laminograph and are responsible for confusing the viewer perception. So unless we have a laminograph and can see the extent to which objects from adjacent planes affect the laminograph of a particular focal plane, we cannot identify the features responsible for strong artifacts. When dealing with flat test objects as in Project No. 1, it is practical to make a laminograph and then remove the artifacts. As a matter of fact the laminography technique itself is used for artifact reduction. The approach is very simple; instead of making a laminograph of the desired focal plane we make the laminograph of the focal plane that contains the features responsible for artifacts. The laminograph enhances these features and using the laminograph the intensity of these features is set to the average background intensity, hence making them disappear. Once the undesired

features are absent from each radiograph another laminograph of the desired focal plane is made, which is free from artifacts (Hsieh, 1999). At first glance we think that this approach makes use of the knowledge gained from a laminograph for artifact reduction, but if we look closely we see that even for this approach the undesirable features are identified before the laminograph formation. Before making a laminograph, the user has to identify the focal plane that contains the artifacts so that the features in that plane can be aligned to make a laminograph. Therefore a priori knowledge of the test object is required for artifact reduction.

When dealing with objects that have complex geometry the approach of making a laminograph of the artifacts to reduce their intensity to background cannot be used. The reason is very simple; this approach can only be used where all the unwanted features are in the same focal plane. An example of such a test object is a two sided printed circuit board (PCB). A two-sided PCB is a flat object with copper conductors running on its two sides, namely the top surface and the bottom surface of the board. When a PCB is placed flat on the x-ray imaging table both of the sides are parallel to the imaging table. As a result both sides represent two independent focal planes in the final laminograph. There are only two possible laminographs of such a test object. One of the top surface and one of the bottom surface (Hsieh, 1999). While we try to make the laminograph of one side the copper lines on the other side act as the artifacts and vice versa. So instead of making a laminograph of the side of the board that we want to image we make a laminograph of the side that we don't want to appear in our final laminograph. While doing so we capture all the unwanted features in the same laminograph because there are no other features in any other focal plane.

Suppose we are working with a test object that is not as simple as the PCB, such as the test object shown in Figure 11. The image shown is of an aircraft skin part. It is very similar to the test object whose radiographs have been used for this research. We can see just by looking at the image that defining the concept of a focal plane containing the unwanted features is very difficult for such a test object.

When making a laminograph of a particular focal plane we shall have interference from numerous other focal planes, making a laminograph of all these unwanted focal planes is simply not feasible. Therefore the approach we have decided to use is to decide beforehand which features we want and which we don't. Unfortunately, we were not able to get a picture of the actual test object that we are processing for our research but it is an aircraft skin part and very similar to the one shown in Figure 11. The objective of making a laminograph from the eight industrial radiographs given to us was to enhance the corrosion that occurs in aircraft skin parts, especially between two metal surfaces riveted together and around the rivets passing through the metal. The rivet heads can be seen as the circular bolt-like objects in the picture shown in Figure 11. The rivet heads conceal most of the corrosion around them so for our research we decided to reduce the images of these rivet heads from the final laminographs. This strategy worked very well as will be shown. Since all else is homogenous metal, only the rivets are responsible for introducing the most unwanted artifacts. Hence the images of the rivets will be reduced in the radiographs and as a result the final laminograph will be clear of artifacts. We next describe the artifact reduction scheme that includes the preprocessing steps, the actual rivet removal scheme, and then the final alignment scheme for laminograph formation.

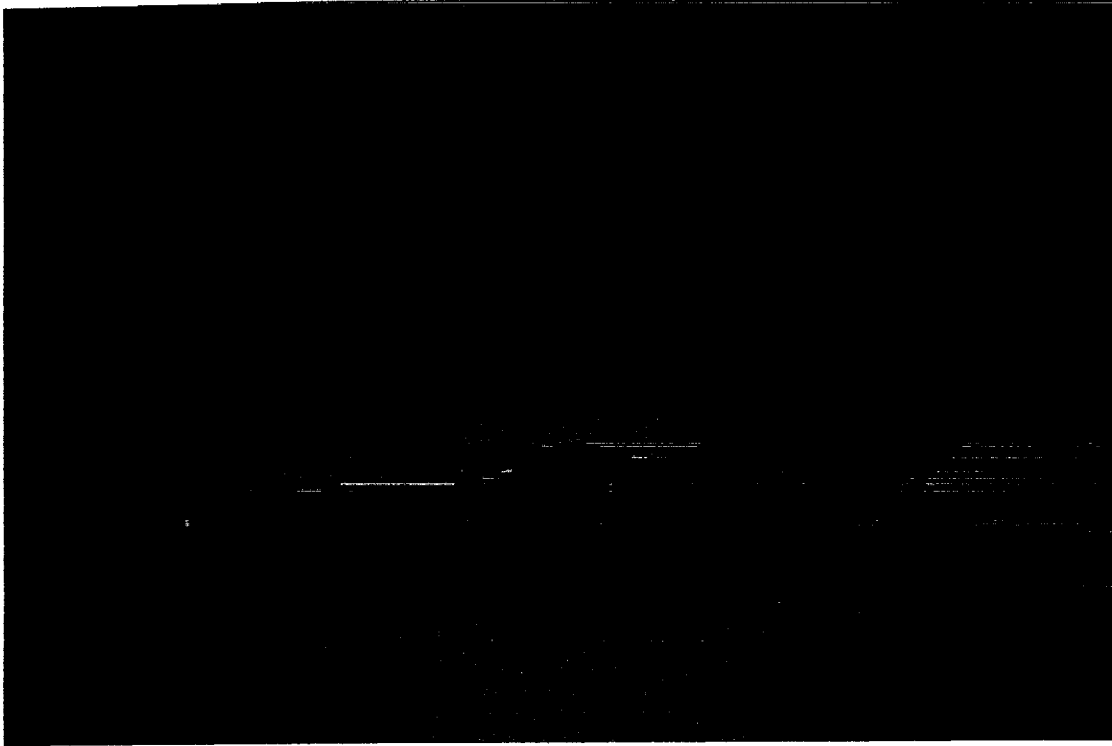


Figure 11. A complex test object

To understand the reason why we chose a region of interest in a radiograph and then processed only this region to make a laminograph refer to Figure 12. It shows an approximate side view of the test object shown in Figure 11.

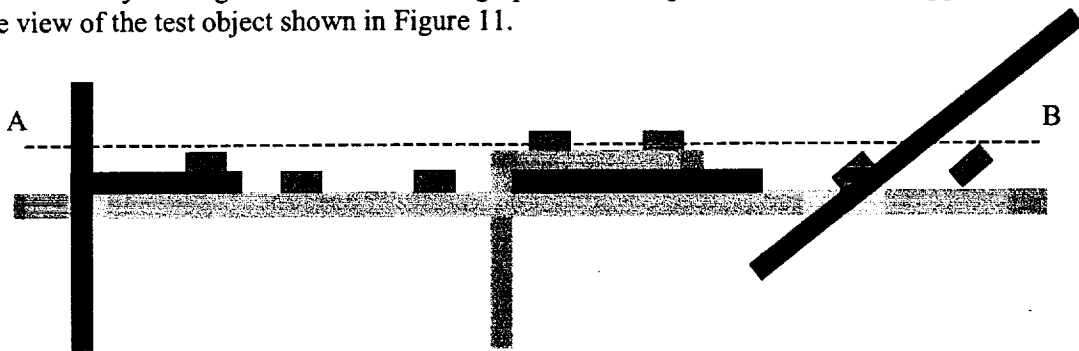


Figure 12. Side view of a complex test object

We are interested in the areas around the rivets, especially under the rivet heads, since we are looking for corrosion. Line AB represents a focal plane, we can see that only two rivet heads are included in this focal plane and most of the focal plane passes through air. So instead of processing the whole image, we subdivide the whole image into subimages and as a result we get more meaningful laminographs with less artifacts from the planes that are adjacent to the portion of line AB passing through air.

This technique has two advantages, first we remove most of the strong artifacts and second, by reducing the image size of each radiograph, we considerably reduce our processing time. For the test object that we have used for our research, the images of rivet heads are very strong. Also the

radiographs are such that just by looking at them one can identify the relatively planer regions. Using the radiographs and our prior knowledge of the test object we subdivide each of the original radiographs into smaller images where each of the smaller images corresponds to a plane area in the radiograph. The eight subimages taken from the eight given radiographs corresponding to approximately the same area are then used for further processing to make a laminograph of that particular region.

Rivet removal.

Two sample images out of the set of eight that we processed are shown in Figure 13. The dotted lines indicate the sections of the images processed separately. The lower regions of the images contain blurred images of rivets (dumbbell shaped) out of the plane of the dotted boxes.

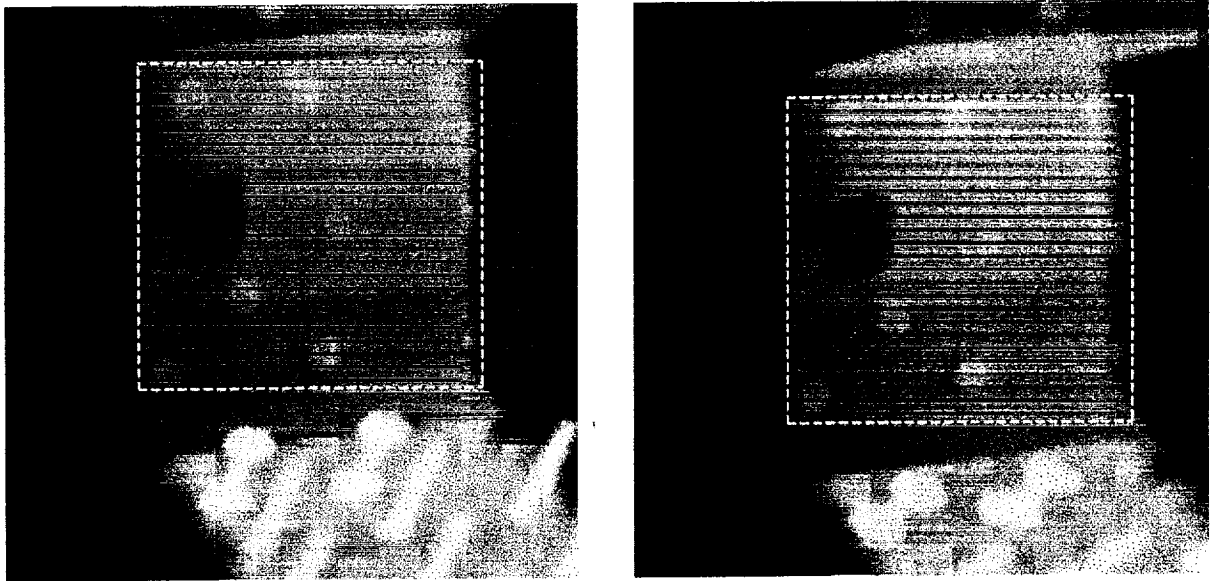


Figure 13. Two of the eight images processed with boxed regions processed separately.

The image enhancement technique we applied here is histogram equalization, one of the most basic operations in image processing. It worked well here. We then applied adaptive Weiner filtering and the Canny edge detector to define the rivets in the images.

Once we get the edge images we can use them to remove artifacts. The method for artifact reduction described is not only good for rivet removal it can be used for artifact reduction for radiographic images in which the desirable features are so weak that they do not appear in the edge map while on the other hand the unwanted features have strong edges. For our case we have the radiographic images of an aircraft skin part. We are looking for corrosion in our test object and we want to get rid of the cloud-like artifact, which is a result of the rivet head images. The corrosion that we are looking for has such a weak image that it cannot be seen without image enhancement. On the other hand the rivet heads have a strong image which can be easily identified from their edge map. At first it looks very frustrating since there is no way that we can make the corrosion image strong without making the rivet head images even stronger. We can make this property work to our advantage if we can use the edge images to obtain a map of the unwanted features, namely rivets.

We want to use binary edge images and manipulate them in such a way that we get a binary image in which the white pixels show the positions of the pixels in the rivet head. The edge

images of the rivet heads are circular ring-like objects with the white pixels showing the perimeter of the circle. We fill the interior of the circle with white pixels. We do this by repeatedly applying dilation and erosion, and then follow this with a region-filling procedure.

The results appear as shown in Figure 14. These two binary images with white spaces in the rivet regions correspond to the two dotted boxes in the images shown in Figure 13.

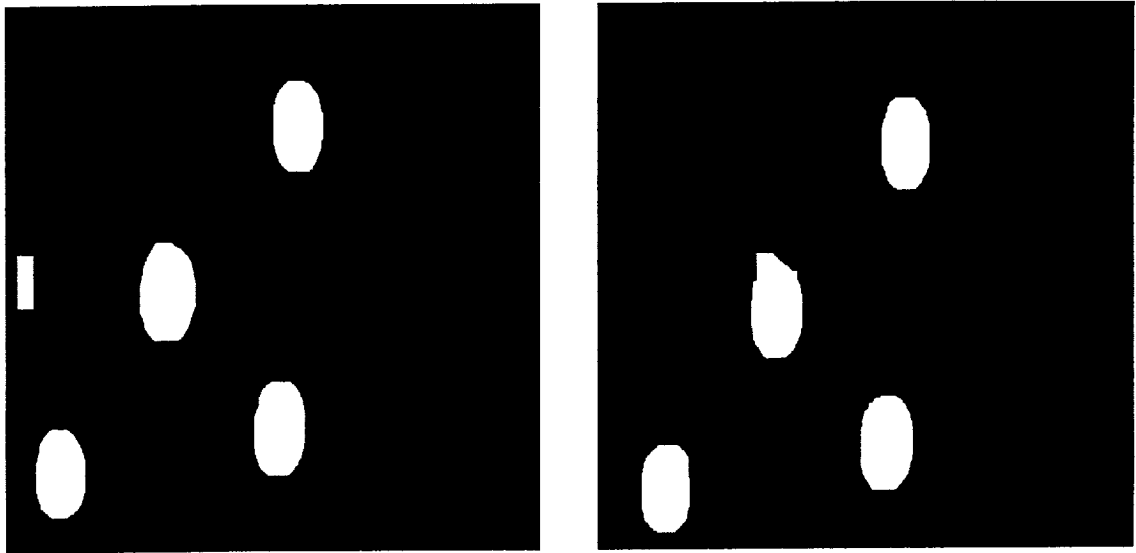


Figure 14. Filled rivet regions determined from the rivet locations in the boxed areas in Figure 13.

Once we have filled up the interior of all the rivet head images in the eight radiographs we use these images to remove the rivet heads from the radiographs.

Erasing Objects

The binary images obtained after region filling give us a complete map of the pixels that are included in the rivet heads. The simple rule is that if a pixel is white in the binary image then it is included in the rivet head otherwise it is not a rivet head pixel. Our goal is to make the rivet heads *fade* into the background or in other words to erase them. If the background were uniform or even gradually changing our task would be very simple. All we have to do is to obtain the average background value and set the rivet head pixels to this value. Unfortunately for our images, the background is rapidly changing and there is no way that we can set all the unwanted pixels to a single value and make them disappear. We decided a type of local averaging, which gave good results.

As a first step in eliminating the rivets, we applied a spatial averaging filter to the gray scale images. These are the original images obtained by the preprocessing steps of cropping, enhancement and noise reduction. The filter is solely used for the purpose of blurring.

Once we get the blurred image we proceed to the next step which makes sure that only the rivet heads are blurred while the rest of the image remains sharp. Once we have the blurred gray scale images, the binary images representing the rivet head pixels, and the original images, we can use them to blur only the rivet heads. The procedure is as follows:

Compare the binary image with its corresponding original and blurred gray scale images. For all the pixel positions corresponding to white pixels in the binary image, replace the pixels in the original image by the pixels from the blurred image. As a result only the rivet heads in the original image will be blurred while the rest of the image will remain sharp. Repeat this process for all the eight images. We get a new set of eight images with only the rivets blurred. Now we take this new set of images and replace the original images with these new images. We then start all over with the adaptive smoothing filter and repeat the entire sequence of steps. The entire process is iterated many times, each time replacing the previous image with the new one in which the rivets are more blurred. After a number of iterations we get an image in which the rivet heads are so thoroughly blurred they are almost invisible. The user decides the extent to which we want to make the rivet heads invisible.

Final laminograph.

The result of this iterative process is shown in Figure 15. Once satisfactory results are obtained, we get a final set of eight images in which the rivet heads are invisible. We use these eight radiographic images for alignment and by properly aligning them make the final laminograph, which is free from artifacts that are due to the rivet heads.

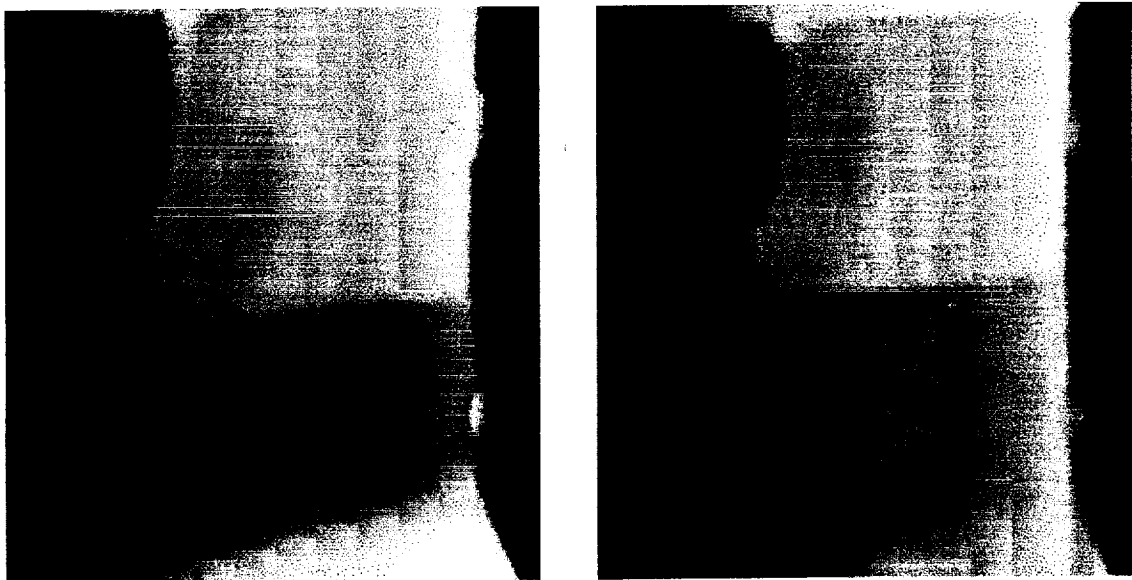


Figure 15. Final radiographic images with the rivets removed. Corrosion can be seen in the center regions of the images.

To illustrate the effectiveness of the rivet reduction, observe Figure 16. On the left is a laminograph made from the original radiographs. On the right is a laminograph made from the rivet-reduced images. Mathematics given by Hayee (2000) can be used to get the depth of the corrosion shown in the central region of the images. Another example of processing a cropped region containing the dumbbell projections of the rivets (see the lower regions in Figure 13) is given by Hayee (2000).

For complete details of all processing steps in Project No. 2, see the MS thesis by Hayee (2000).

Conclusions

The proposed artifact reduction scheme works well for the test object under consideration for this research. This scheme gives a good format for artifact reduction in laminographs of volume test objects. Whereas Project No. 1 for flat object depended on a single average gray level value for background, the scheme proposed in Project No. 2 depends on local background gray level around each artifact. By taking the average gray level locally we were able to skip the background trend removal, which is an essential part of most of x-ray image processing. By avoiding trend removal most of the image contrast can be preserved.

The scheme developed should work equally well for other complex test objects, in which the main goal is to locate corrosion. The shift that is required in each radiograph gives useful information about the depth of corrosion. The knowledge about the exact shift in detector position and each radiograph is enough to calculate precise corrosion depth.

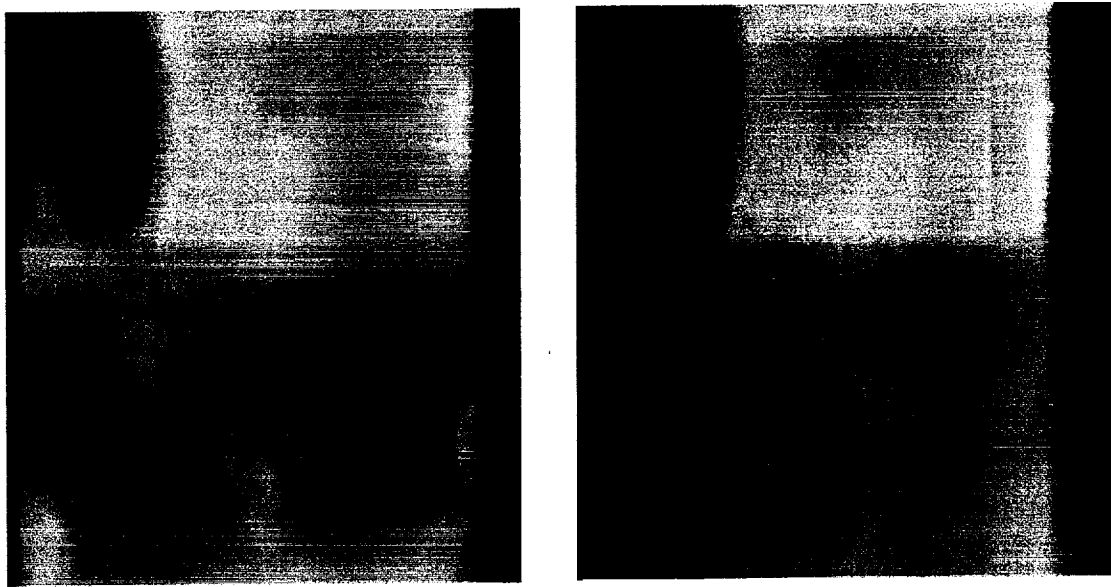


Figure 16. Laminographs of the original radiographs (left) and of the images processed to remove rivets (right).

Additional techniques can be applied to improve this scheme. First of all the process should be made completely automatic with no user interference. Currently the user has to specify the center of each rivet to start the region filling while making a binary map for the positions of the pixels forming the rivet head. Also the focal feature selection for the alignment procedure is also user defined. The operator has to choose the focal feature in each radiograph by using the cursor. This kind of human intervention always introduces errors. Complete knowledge of the geometry of the imaging system can help in making the alignment procedure automatic.

Once an image is divided into sub-images, each set of these sub-images is processed separately. An ideal situation would be where we can segment the image into smaller images, make a laminograph of each smaller area and put the final laminograph of each region together to make a single laminograph of the original image. It is not possible in the scheme proposed here because for each set of sub-images, a focal feature is defined which can be identified in all images. The focal feature can be at different depths for different sets of sub-images. In other words we can

say that the focal plane enhanced in each laminograph is different. The smaller laminographs can only be put together when they show the same focal plane. Since there is no way that we can ensure this, therefore it is not possible to put the smaller laminographs together to make a single laminograph of the whole image.

The necessity to make a single laminograph of the whole object depends on the kind of object that we are imaging. If the test object is a printed circuit board and we are looking for breaks in copper conductor lines, then it is necessary that we have one laminograph of the whole PCB because we don't want to miss any breaks in the copper lines. While imaging corrosion, if smaller laminographs of different areas are formed and boundary of corrosion can be identified in one of these smaller laminographs then this smaller laminograph yields all the information that is required by the user and it is not necessary to make a single laminograph of the whole test object.

References

Canny, J. "A Computational Approach to Edge Detection," IEEE Trans. Pattern Analysis and Machine Intelligence, vol. 8, pp. 14-20, Jan. 1998.

Hsieh, H.-C., "General Artifact Reduction Scheme for Laminography," unpublished MS Thesis, Iowa State University, Ames, IA, 1999.

Hsieh, H.-C., and Basart, J. P., "General Artifact Reduction Scheme for Laminography," Review of Progress in Quantitative NDE, D. O. Thompson and D. E. Chimenti, eds., Vol. 18A, pp. 765-771, Plenum Press, NY, 1999.

Hayee, S., "Laminography: Artifact Reduction Scheme for Objects with Complex Geometry," unpublished MS Thesis, Iowa State University, Ames, IA, 2000.

Hayee, S., and J. P. Basart, "Artifact Reduction Scheme for Objects with Complex Geometry," Review of Progress in Quantitative NDE, D. O. Thompson and D. E. Chimenti, eds., Vol. 19A, pp. 725-732, Plenum Press, NY, 2000.

Appendix

Calibration Procedure for XRSIM Beam Model

Calibration Procedure for the X-ray Generator Model in XRSIM

Background

There are a number of parameters that describe the performance of a typical industrial x-ray generator. These parameters include the power loading on the target, P_{\max} , the maximum kilovoltage, V_{\max} , the selection of the operating kilovoltage, kev , the electron beam current, mA , the target material, X_t , the angle that the target surface makes with the electron beam, θ , the vacuum window material, X_{win} , and intensity scale factor, etc. There are several data tables, built into the code, that provide the bremsstrahlung production cross section for the production of one photon from the interaction of the relativistic electron with the bound electron in the target material. The second table included in the bremsstrahlung module is the energy loss that an electron experiences as it decelerates via a coulomb interaction with the target electrons.

The bremsstrahlung model in XRSIM is based on a thick target bremsstrahlung model where all of the electron energy is either deposited as thermal heat in the target material or is converted into a bremsstrahlung photon. Since electron accelerated to the typical energies used in industrial radiography are relativistic, relativistic effects must be included into the model. Further, the electron beam interaction is with the bound electrons in the target material, meaning that the interaction cross section must include the electron wave function of the bound electron. This overlap integral becomes quite complicated and requires the use of numerical solutions. This was first done by Pratt, et al. (1) This treatment is the first attempt to correctly account for the physics of thick target bremsstrahlung production. Previous treatments usually are based on a non-relativistic classical treatment first done by Kramer(2) in the early 1920's.

The result of the above treatment correctly provides for the description of the high energy end of the bremsstrahlung spectrum, namely up to the maximum photon energy, where all of the electron kinetic energy is converted into a bremsstrahlung photon. The low energy behavior in reality is quite different in that at low energy the photon production also drops to zero. This low energy behavior is due to the inherent filtration of the tube. There are two components to this, the first is the filtration resulting from the vacuum window material, and the second is the filtration from the target itself. The electron beam penetrates into the surface of the target resulting in the production of bremsstrahlung photons within the target material. These photons are then subject to the same attenuation through the target material as they are through the vacuum window. The penetration depth, δ , is calculated using the Thomas-Widdling constants(3) and is dependent on the energy of the incident electron. The appropriate attenuation length out of the target is dependent on the angle that the electron beam makes with the face of the target, the attenuation coefficient used is dependent on the material of the target.

These two pieces, the proper bremsstrahlung production cross section and the calculation of the inherent filtration, generate the familiar shape of the typical industrial tube spectrum. The characteristic lines from the fluorescences of the k and l shell electrons in the target are also included, although they have a small effect to the overall model.

Calibration

To calibrate the XRSIM bremsstrahlung model to a particular generator, several things must be done. Examination of Table 1 shows the input parameter file for the generator description. The correct values for these parameters need to be entered. The last entry is a calibration factor. This has been included, as it is sometimes difficult to determine the angle, θ , from the manufacturer equipment specifications. The following outlines the procedure used at the Center for NDE to determine the calibration factor.

Since the spectrum generated by an x-ray tube is a white spectrum, we used an energy dispersive detector. There are a large number of these types of detectors including germanium, NaI, CdTe, and CdZnTe to name a few. To be effective these detectors must have appropriate energy resolution. The germanium detector has the best resolution and is the one of choice used at the Center. The disadvantage to the Ge detector is that it must be cooled in order to operate. Typically this is done using an LN₂ bath with a dewar providing a supply. The detector is attached to a multi-channel analyzer (MCA) system that provides the photon counting and the energy discrimination. The basic idea of these detectors is that an x-ray photon deposits its energy in the detector material with the result being a voltage proportional to that deposited energy. The pulse height analysis provided by the MCA can digitize these pulses from the different x-ray photons. Each energy will result in a different pulse height. The result is a number of counts in various energy or voltage ranges. The use of an isotope calibration source set allows for the conversion of a channel number into a photon energy. We typically use calibration sources of Co⁵⁷, Am²⁴¹, Cs¹³⁷, and Cd¹⁰⁹.

The key features include a shield around the detector, a pinhole collimator allowing the x-ray generator flux into the detector, a source, and a source to detector distance. The purpose of this measurement is to obtain the number of photons per keV per steradian per second. To do this we need to know the distance from the source to the detector and the size of the collimator aperture. The collimator hole for our detector is typically 300 microns in diameter in a 0.25-inch lead plate. The shielding is typically 0.25 inches of lead, although 0.125 inches of tungsten can be used. Some care needs to be taken in aligning the pinhole with the center of the source. This resulted in a detector being placed on a computer controlled motion table with x-y-theta control. This leaves only one degree of freedom not easily controlled, namely, the vertical tilt. The reason for this care is that if the collimator hole is lined up as a cat's eye, the actual solid angle subtended by the aperture will be over estimated and the resulting flux too low. The alignment of the aperture in the collimator can be aided by the use of a laser. Generally it is done by systematically varying the two translation degrees of freedom and the two rotational degrees of freedom. This process can be tedious taking several hours to do.

Once the collimator is aligned, spectrums are measured at a low energy, a mid range energy and a high energy. Care must be to make sure that the MCA electronics are not saturated; this can be determined by insuring the dead time of the MCA isn't over 15%. The signature that the dead time is too high or that the number of photons being counted are in error is whether the measured spectrum has photon events higher than the set kilovoltage on the generator. If there is a noticeable amount, then there are sufficient numbers of photons arriving that two simultaneous photons of lower energy are being counted as one photon at a higher energy. This problem is most apparent at the high kilovoltage settings. The alternative is to increase the source to detector distance or to reduce the aperture size.

The results of these measurements are plotted with the results of the bremsstrahlung output. The calibration factor is the multiplicative scale factor that matches the peak of the bremsstrahlung spectrums. This number need only be computed for one energy and then entered into the xr_gen.dat setup file. One other factor is sometimes required. This occurs if the low energy portion of the spectrum doesn't match or if the target angle is not known. The inherent filtration isn't computed properly. We adjust the location of the low energy cutoff by adjusting the target angle. This is then followed with the intensity calibration.

Equipment needed

- energy dispersive detector
 - Ge Ln₂ cooled or a cooled CdZnTe detector
- pulse height analysis equipment (MCA)
 - high voltage supply
 - amplifier
 - MCA
 - counter timer
 - power
- collimator

300 micron diameter
detector shielding
0.25 " of lead

Alternative Calibration Method

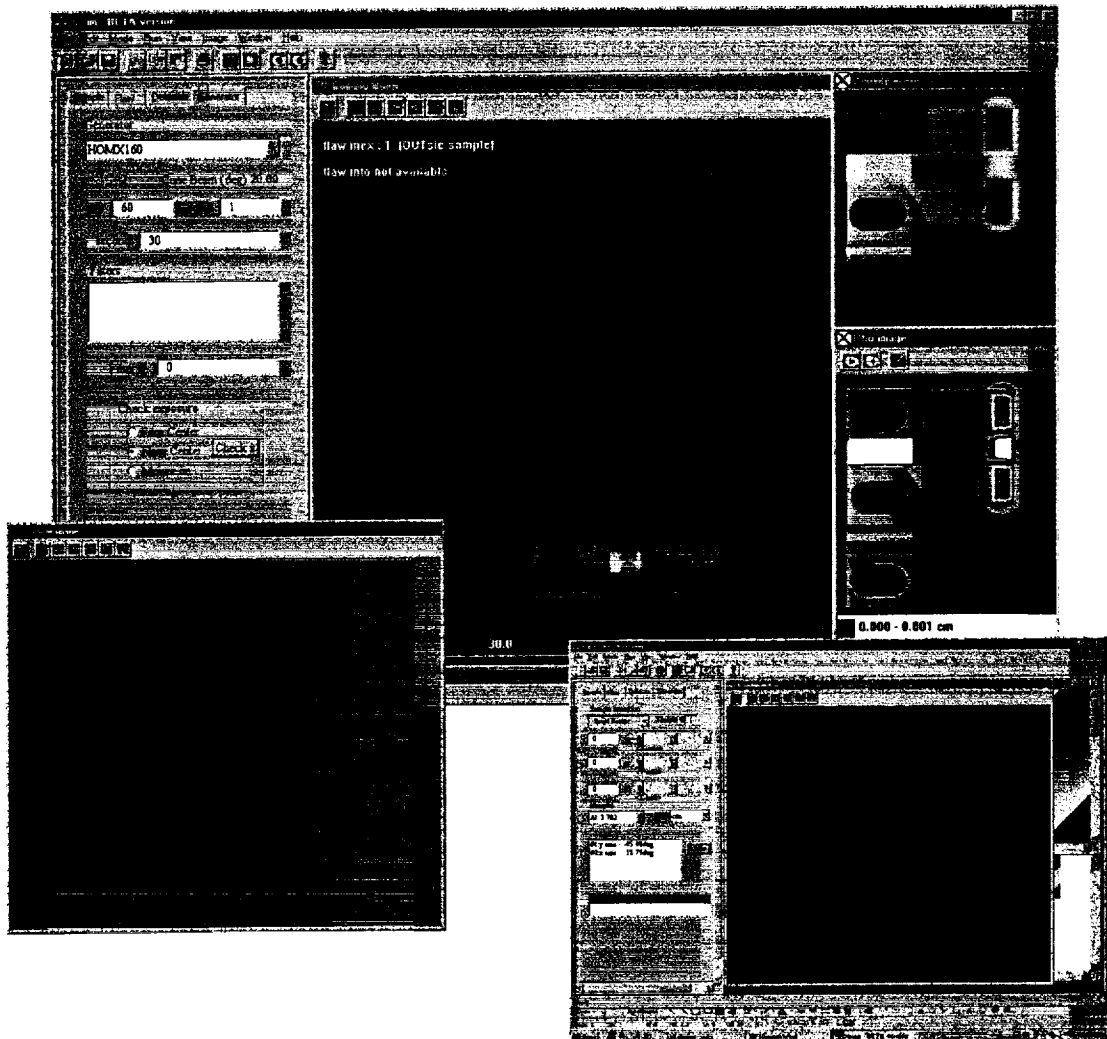
We have developed an easier, although approximate, method of x-ray generator source calibration recognizing that the above procedure is not always possible. Often the proper equipment is not available or a key piece of information is not known. The procedure for this method involves using several plates of material ranging in thickness from 0.25" to 1". We are presently using aluminum. At low kilovoltage, for example 140 keV set an exposure time for 0.25 and 1.0 inches of aluminum to achieve a density of 2.5. Using the same parameters used in the experimental set up calculate the film density for a plate with the same thickness of the same aluminum alloy used in the experiment. Adjust the scale factor until the density calculated with XRSIM matches the observed density on the film. If the film developer is properly adjusted and the default inherent filtration is reasonable close, we have has good results with the procedure.

Table 1 An example of the input parameters for a typical x-ray tube as used in XRSIM.

```
* file xr_gen.dat
* x-ray generator model
#####
####
%
HOMX160
*
* target material (properties to be read from material property
datafile)
W
*
* target angle (deg.)
45.0
*
* window material (properties to be read from material property
datafile)
Al
*
* window thickness (cm)
0.05
*
* collimation of cone beam (deg.)
20.0
*
* generator maximum kV
360.0
*
* generator maximum power (Watts)
2750.0
*
* intensity normalization factor (from calibration data)
1.0
*
```

XRSIM

USERS MANUAL



Center for Nondestructive Evaluation
Iowa State University
3/01

INTRODUCTION TO THE X-RAY SIMULATOR (XRSIM)

The X-ray simulator (XRSIM) program was designed and developed at Iowa State University's Center for Nondestructive Evaluation. The program simulates radiographic inspections using a computer aided design (CAD) model of a part to produce physically accurate simulated x-ray radiographic images. The program allows the operator to select different parts to inspect, adjust the placement and orientation of the part to obtain the proper equipment/part set-up, and adjust all the usual x-ray generator settings to arrive at the desired radiographic film exposure.

Successful radiography depends on numerous variables that affect the outcome and quality of an image. Many of these variables have a substantial effect on image quality and others have little effect. Using the XRSIM program the inspection variables can be modified and the resulting image viewed and evaluated to assess the impact that these variables have on the image. Many inspection scenarios can be rapidly modeled since the shot set-up and exposure can be quickly accomplished and the film-developing step is eliminated. The almost instantaneous results are especially valuable in education and training settings. Not only can a greater number and variety of problems be explored, but also the effects of variables can be learned by self-discovered through experimentation, which is one of the most effective modes of learning. Also, the results are not complicated by unnecessary variable such as film processing artifacts, and many of the distractions unrelated to the primary learning exercise (that can confuse the results and even the purpose of the exercise) are eliminated. Using the program, a more effectively understanding of the scientific concepts associated with radiography will be developed.

Another important aspect of the program is that it does not require a real part for the inspections. Inspections can be simulated that would otherwise be impossible or too costly to perform outside of the computer environment. Flaws of various shapes and sizes can be easily introduced into the CAD model to produce a sample set for probability of detection exercises. Caution must be used when applying the results, as densities produced in the simulated images may not match exactly the images produced in the laboratory using similar equipment settings. The difference between the actual and simulated radiographs is primarily due to approximations made in the scattering model in XRSIM. To keep the computation times reasonable, we have simplified this part of the model. As scattering effects become more dominant, for example a 1" steel sample at 250 kVp will have over half of the total flux reaching the detector be due to scattering, the predicted density will agree less with the actual density on the radiograph.

The XRSIM program has been designed to run in a Windows® environment on an IBM or IBM compatible, Pentium II computer. It is assumed that the user is familiar with the Windows® operating system and its standard features such as pull-down menus and toolbar buttons. These instructions will explain the basic steps for producing an image using the program.

STEPS FOR PRODUCING A SIMULATED RADIOGRAPH

The steps required to produce a simulated radiograph using XRSIM are basically the same as those required to produce a true radiograph. The only required extra step involves generating a 2D-thickness map of the part CAD file once the part has been positioned and oriented as desired in the simulated x-ray vault space. A second extra step that may be included in the XRSIM procedure is to introduce a flaw into your sample (flaws are optional when using XRSIM). The steps required to produce a simulated radiograph are:

1. Open the XRSIM program.
2. Select a sample (CAD file) to radiograph.
3. Position and orient the sample relative to the film and x-ray tube.
4. Select the material of the sample.
5. Introduce a flaw into the sample, if required.
6. Run the CAD function to produce a 2D-thickness map of the sample.
7. Select the desired film.
8. Resize and reposition the film to image the desired area of the sample.
9. Select the x-ray generator to be used.
10. Set the kilovoltage, amperage and exposure time of the generator to the settings required to produce the desired radiographic image.
11. Run XRSIM (expose the film) to produce the simulated radiograph.

These instructions are broken into two sections. The first section covers the basic operation of required to produce an image. The second section covers some of the less used features of the program. Topics covered in this second section include:

1. Working with multiple samples and flaws
2. Resizing the part.
3. Modifying the resolution of the image.

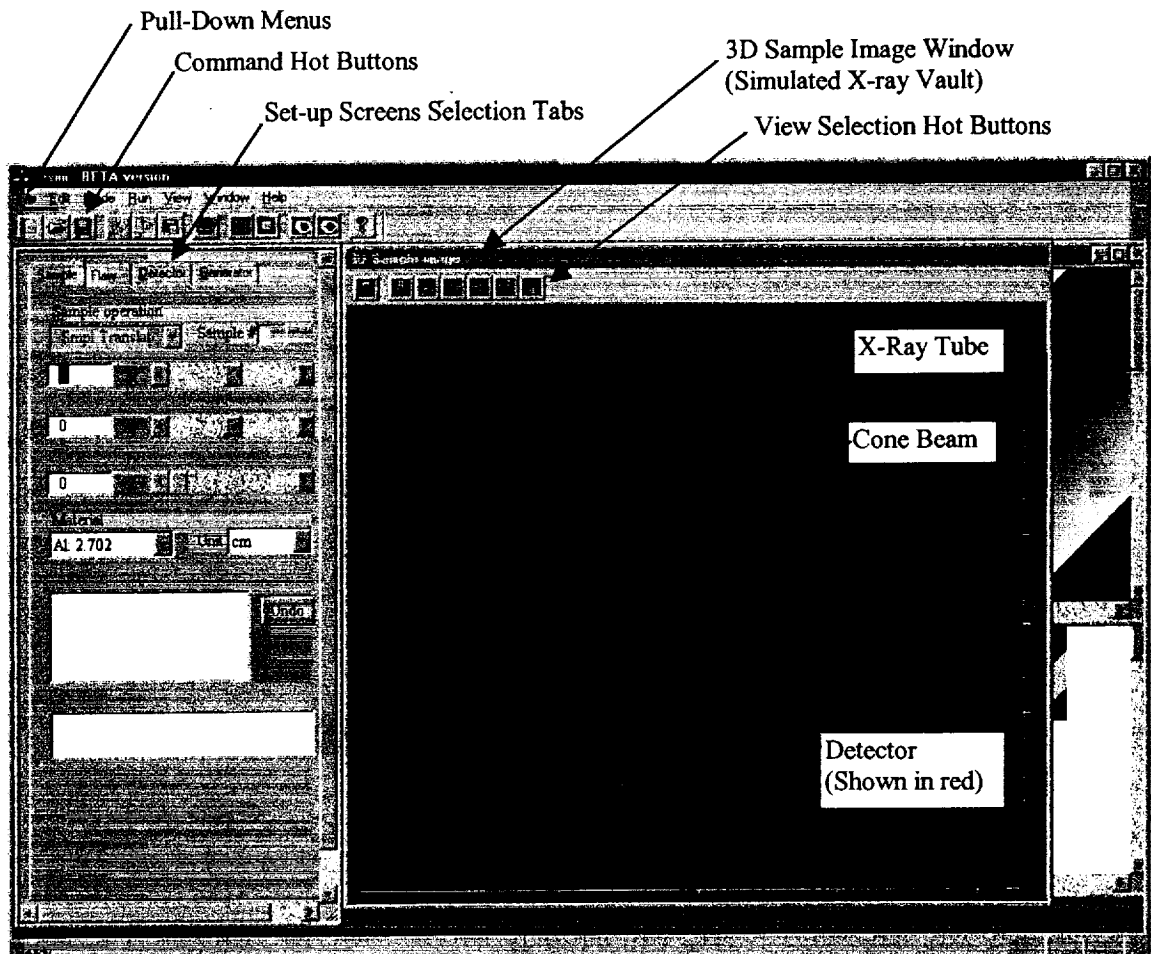
SECTION 1- BASIC OPERATIONS

OPENING THE SIMULATION PROGRAM

1. Find the XRSIM.exe program file on the computer.
2. Double click on the XRSIM icon.

FINDING YOUR WAY AROUND IN XRSIM

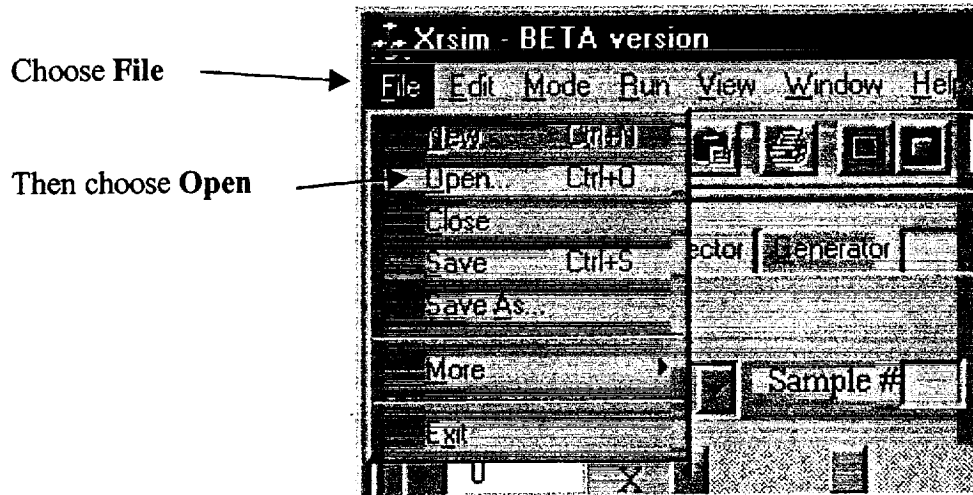
When the program opens, you will see the screen below. At the top of the main window you will pull-down menus and command hot buttons that function the same way they do in any Windows® environment. The command hot buttons provide shortcuts for most of the highly used commands found in the pull-down menus. The controls used to select and modify the sample, flaw, detector, and the generator are separated into four set-up windows. The desired set-up window can be displayed by clicking on the selection tabs provided for each of the windows.



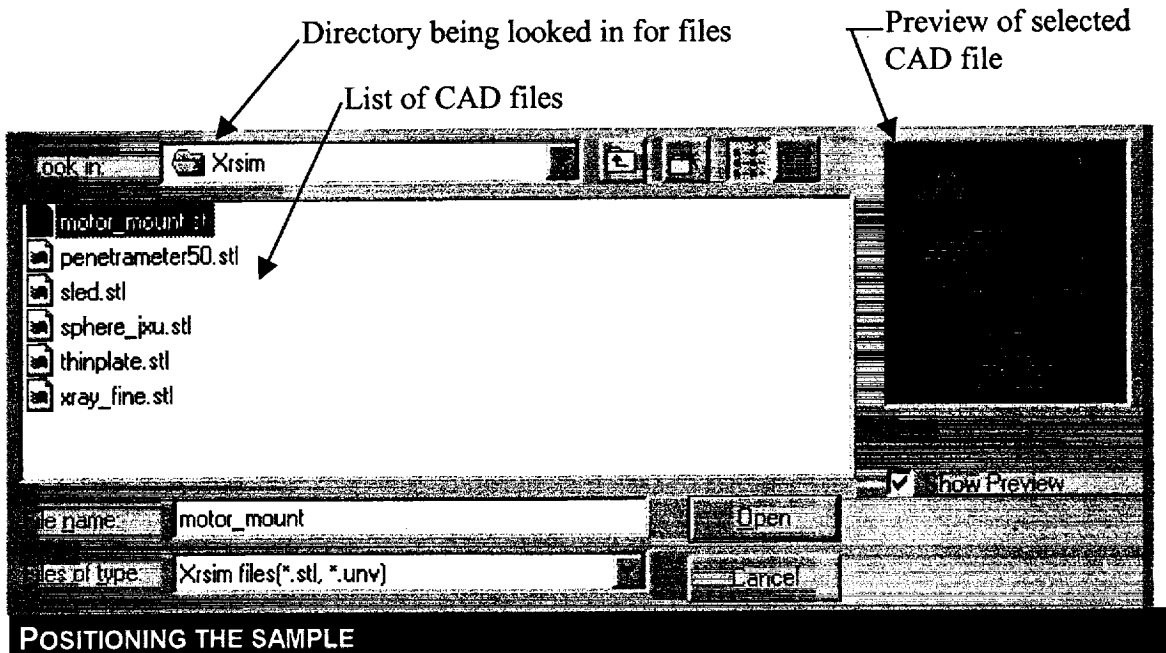
CHOOSING A SAMPLE (CAD File of Part)

When the program opens, the set-up window **Sample** tab will be selected and the **Sample** set-up window will be displayed and active. The first action required is to open the sample CAD file selection window and choose a sample to inspect.

1. In the upper left corner of the screen, choose **File** and then **Open** (or use the file open hot button).
2. You will see a number of part CAD files that may be selected. Double click the motor_mount.stl file or select the file and click on the **Open** button.
3. The selected sample will appear in the **3D Sample Image** window.

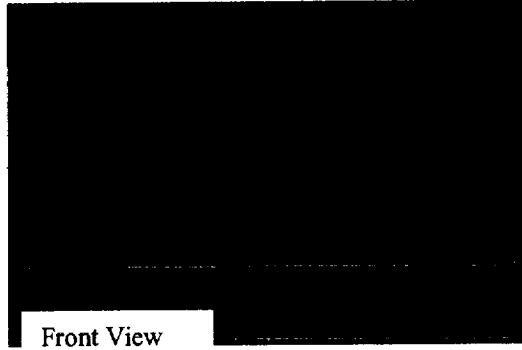
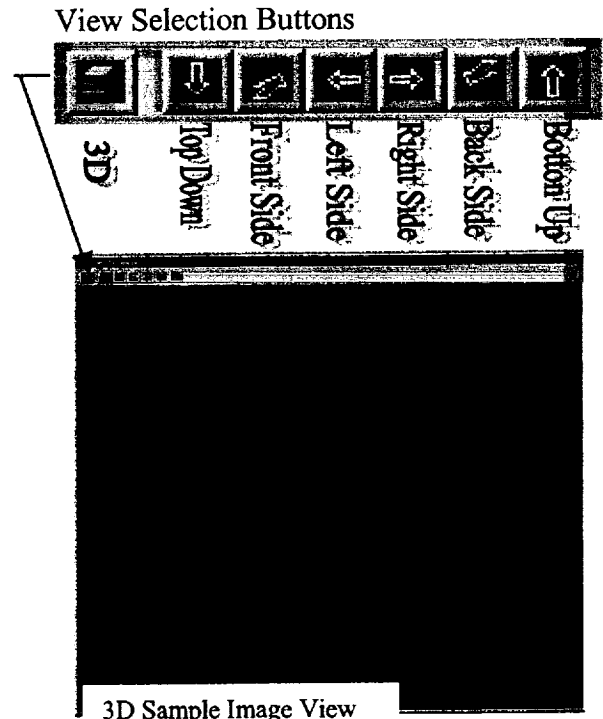
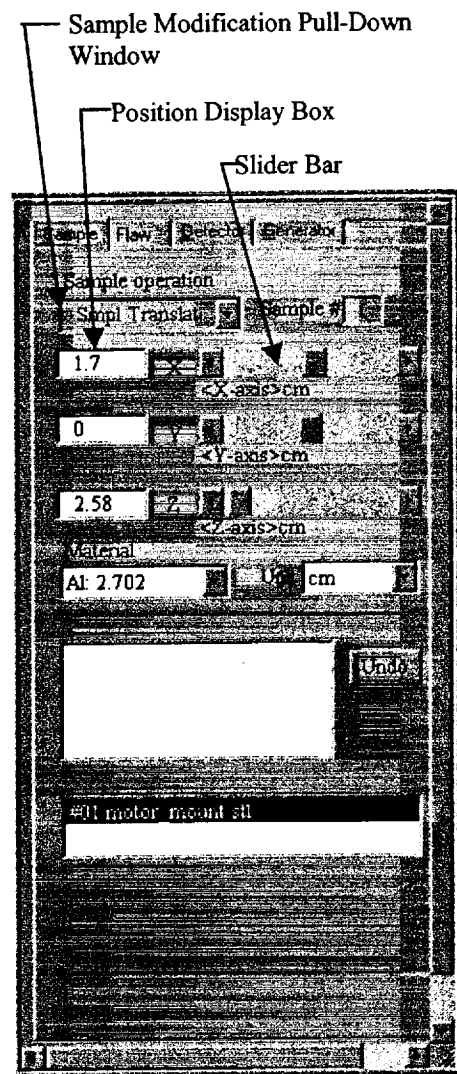


The Part CAD file selection window (shown below) will open.



Once a part is brought into the program, it must be positioned and oriented properly in relation to the x-ray source and the film just as would be required in the x-ray vault. The part will appear green in the **3D Sample Image** window as shown on the right below.

1. Use the view selection tabs at the top of the **3D Sample Image** window to display the part from different views. The part can be viewed in 3D, from the front or back, from the right or left side, and from the top or bottom.
2. The part can be moved in any of three ways. First, the part can be moved by clicking and dragging it in any view. The part will not track as fast as the mouse so stop occasionally to let the part catch-up with the mouse pointer. The part can also be moved typing a number in the position display box (the change takes effect when the enter key is depressed) or by using the slider bar or arrows.



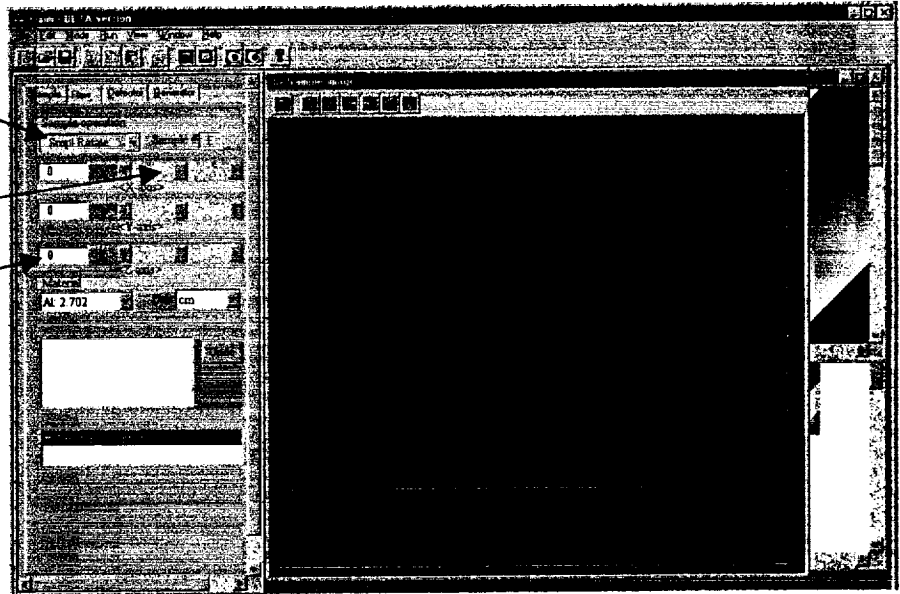
ORIENTING THE SAMPLE

The orientation of the part can also be modified in the Sample set-up window.

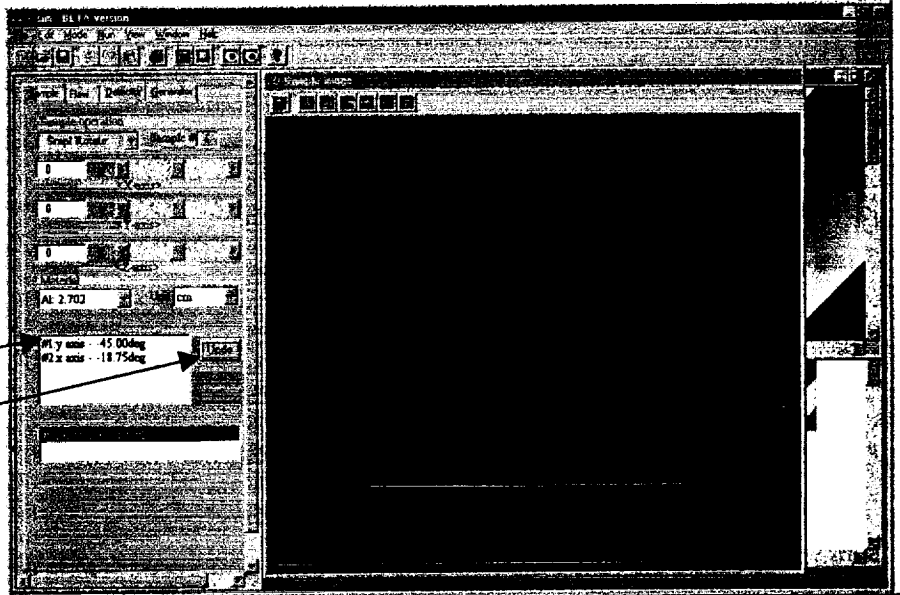
1. In the **Sample** set-up window, choose **Smpl Rotate** in the **Sample operation** input box.
2. Use the slider bars to change the orientation of the sample. When looking at the sample from the front view, the x slider will rotate the sample about an axis that runs left/right, the y slider will rotate the sample about an axis that runs in/out of the screen, and the z slider will rotate the sample about an axis that runs up/down.
3. Any rotation can be easily undone by selecting the operation and clicking the **Undo** button

Select **Smpl Rotate**

Rotate the sample using the slider bars or by typing in a numerical value (in degrees).



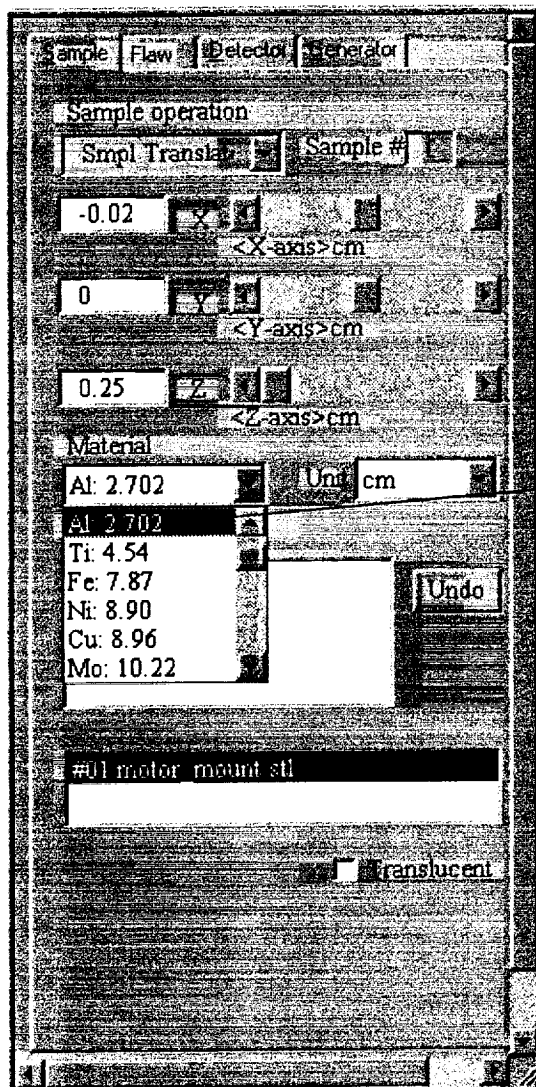
Any of the rotation steps can be undone by selecting the desired step and clicking on the **Undo** button.



CHOOSING THE MATERIAL FOR THE SAMPLE

Two factors effect the interaction of the part with the incident x-ray beam, the material of the part and the density of that material. Lead attenuates a photon of any energy more than aluminum, indicating the effect of the makeup of the atomic number of the material. The attenuation coefficient for a particular energy increases as the fifth power of the atomic number, namely, Z^5 . For some materials, for example, ceramics, the composition of the ceramic material does not change, but the density does. In the case of ceramics, a green state material may have a density of only 60% of the fully fired state. In this case, the linear absorption coefficient scales linearly with the density of the material.

1. Locate the **Material** dialog box near the left-center of the sample window. Select the desired material for the part from the materials listed in the dialog box. The material density (in grams per cubic cm) is provided for each of the materials listed. The materials are further described in Appendix 1.



Select the desired material for the sample Material dialog box on the sample set-up window

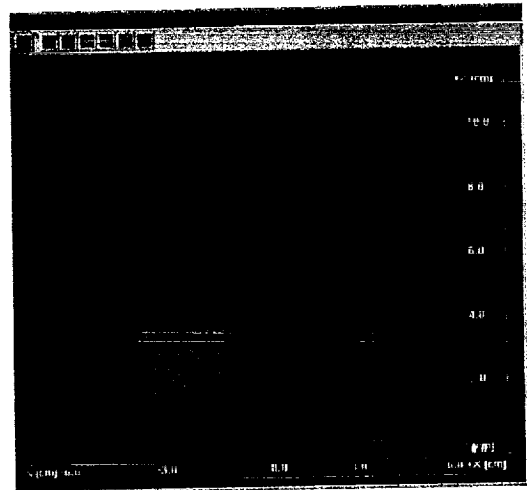
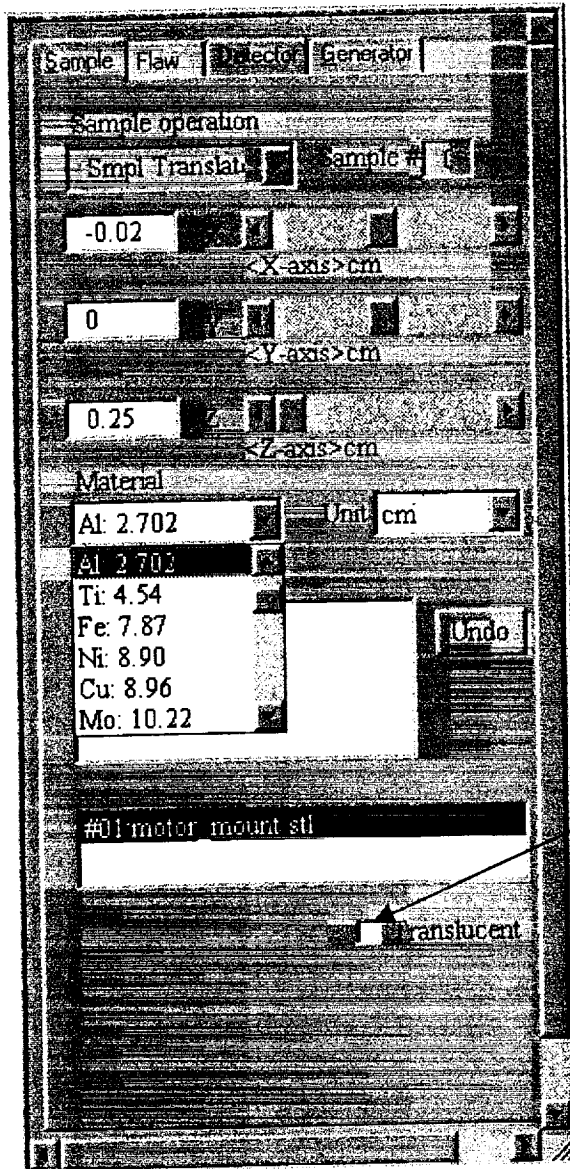
Click on the arrow to display the list of materials available.

Click on a material to make a selection.

DISPLAYING THE PART IN THE TRANSPARENT MODE

The part is normally displayed as a solid 3D model. There are times when displaying the sample in a translucent mode is useful. One of these times is when positioning a flaw in the sample. Using the translucent mode allow the flaw to be seen so it can be imbedded below the surface of the sample.

1. The sample can be displayed in the translucent mode by checking the **Translucent** box near the bottom of the sample window.

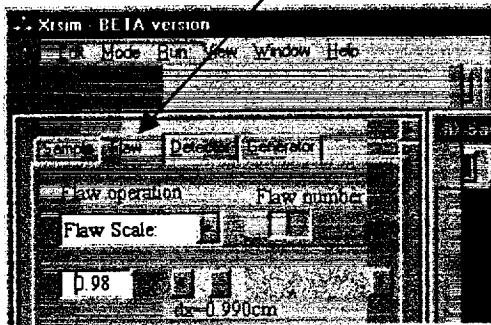


Display the sample in the translucent mode as shown above by checking this box

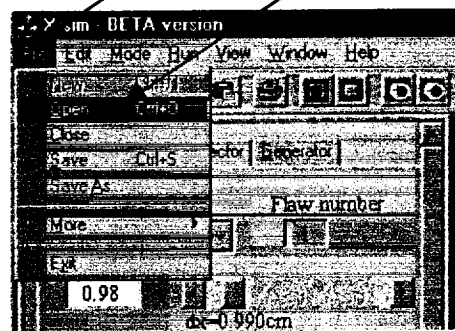
If desired, a flaw may be introduced into the sample. The flaw is a CAD model file (like the sample) so that any flaw configuration can be modeled in the program. Several flaw CAD files of basic shapes, such as a sphere and half sphere, are furnished with the program. These flaws can be resized to roughly represent some of the common material flaws such as voids, semi-circular cracks, and delaminations.

1. Click on the **Flaw** tab to select the flaw set-up window.
2. Open a flaw in the same manner that the sample was opened. In the upper left corner of the screen, choose **File** and then **Open** (or use the file open hot button).
3. You will see a number of flaw CAD files that may be selected. These files have a **flw** extension. Double click the sphere.flw or select the file and click on the **Open** button.
4. The selected flaw will appear in the **3D Sample Image** window.

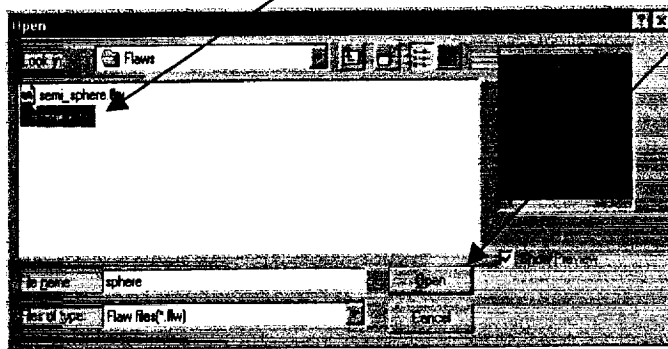
Select the **Flaw** set-up screen



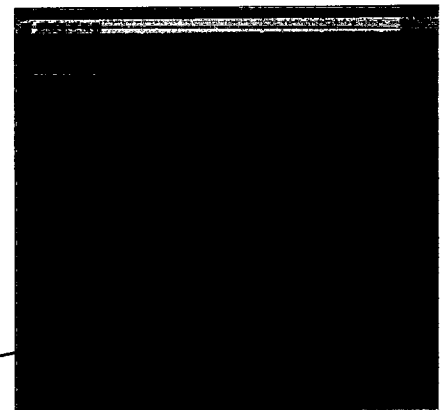
Select **File** then select **Open**



Double click on a flaw file or select the file and click **Open**



The flaw will appear in the 3D Sample Window (front view shown in light green). The location of the flaw from the boundaries of the part is given in the upper



CHOOSING A MATERIAL FOR THE FLAW!

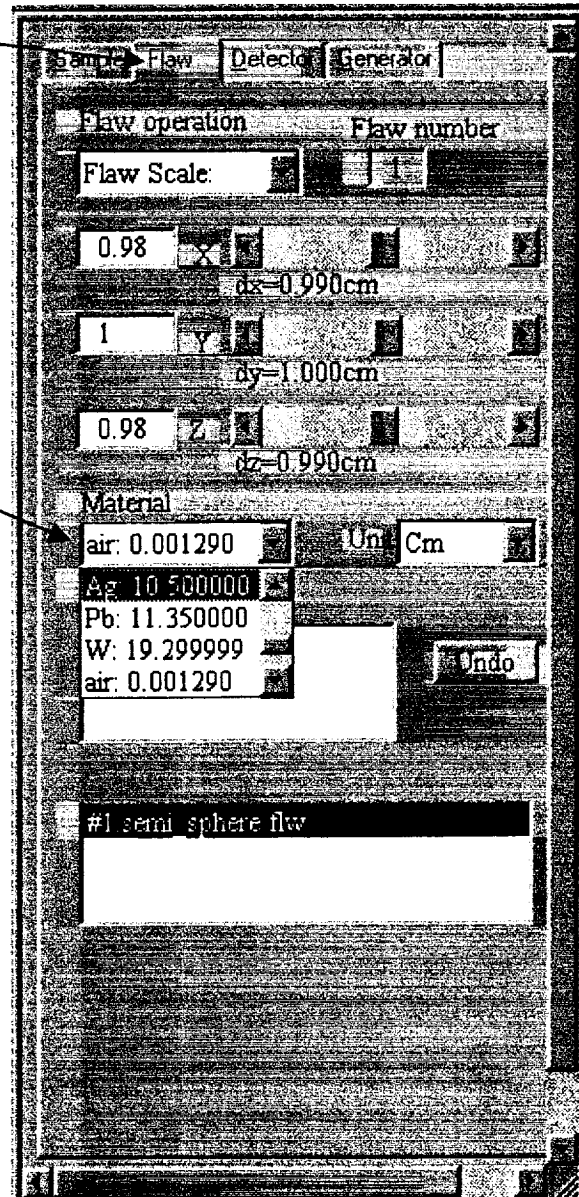
Just like the sample, the flaw can be modeled as any number of materials. Materials representing a variety of densities are available for selection as the flaw material. These

materials include air to represent cracks and voids in the part, and a variety of high and low-density materials to represent inclusions. The materials are further described in Appendix 1.

1. Locate the **Material** dialog box near the left-center of the **Flaw** window.
2. Select the desired material for the part from the materials listed in the dialog box. The material density (in grams per cubic cm) is provided for each of the materials listed.

Make sure the **Flaw** tab is selected

In the **Material** selection dialog box, select the desired material

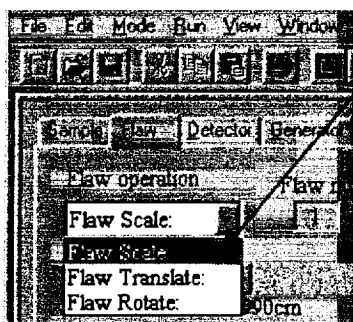


SIZING THE FLAW

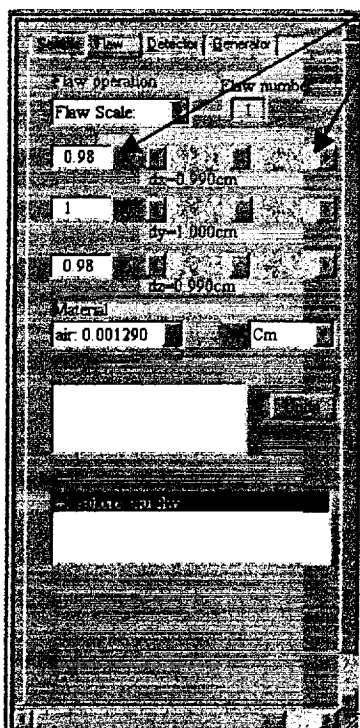
Once a flaw is brought into the program, it must be sized, positioned and oriented properly in the sample. It is usually easiest to size the flaw first, before it is placed in the sample.

A flaw such as a sphere can be resized to represent a delamination by making one of the dimensions very small.

1. Use the view selection tabs at the top of the **3D Sample Image** window to display the flaw from desired view.
2. In the flaw set-up window, choose **Flaw Scale** in the Flaw Operation dialog box.
3. The flaw can be sized by typing a value in the flaw size dialog box (the change takes effect when the enter key is depressed) or by using the slider bar or arrows to change the flaw value. A dialog box and slider bar is provided for each of the three dimensions of the flaw. Therefore, to reduce the size of a flaw such as a void (sphere) without changing its shape, the flaw must be scaled equally in all dimensions.

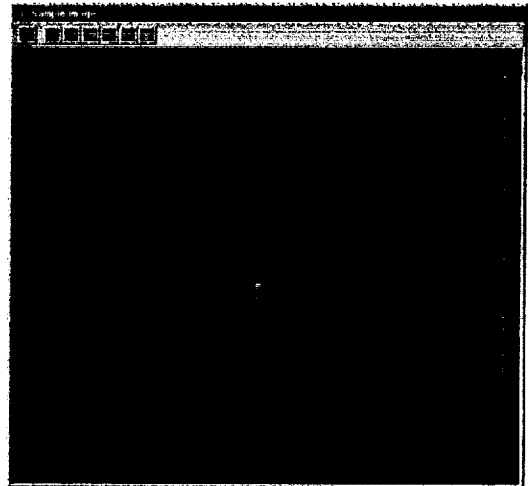
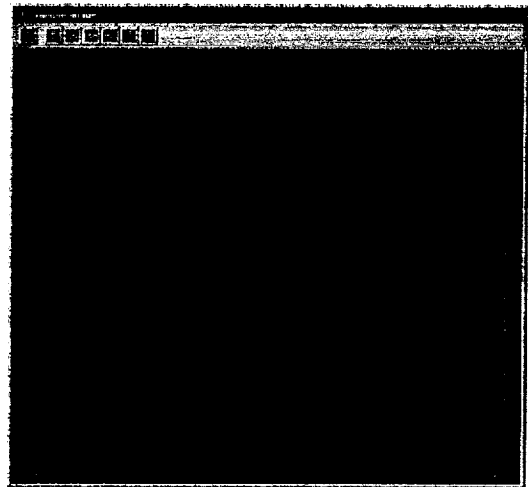


Choose **Flaw Scale** in the **Flaw operation** dialog box in the **Flaw** set-up window



Enter a value in the dialog box or use the slider bar to scale the flaw in the desired dimension

Reducing the value of the X dimension, will change the shape of the flaw shown above-right to that shown below-right



ORIENTING THE FLAW

The flaw is oriented in the same manner that the sample.

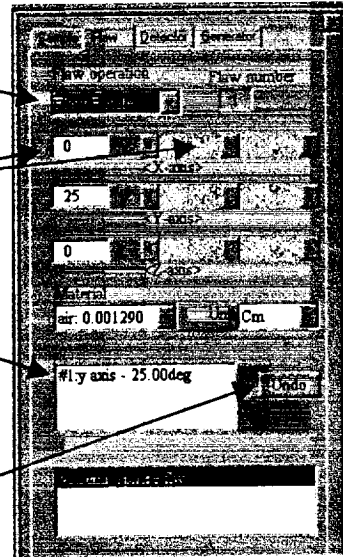
1. Select the **Flaw** tab to display the flaw setup window
2. Select **Flaw Rotate** in the **Sample Operation** dialog box
3. Type a numerical value in the dialog box and hit the enter key or use the slider bars to change the orientation of the flaw. When looking at the flaw from the front view, the x slider will rotate the flaw about an axis that runs left/right, the y slider will rotate the flaw about an axis that runs in/out of the screen, and the z slider will rotate the flaw about an axis that runs up/down.
4. A rotate operation can be undone by highlighting the operation in the dialog box next to the undo button and click on the **undo button**.

Select **Flaw Rotate** in the **Flaw Operation** dialog box.

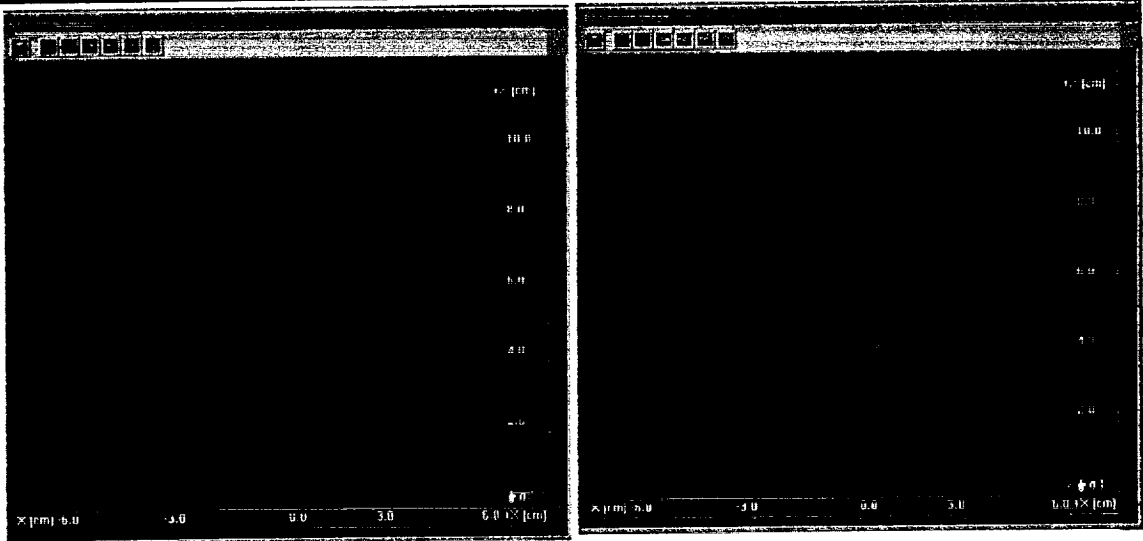
Enter a numerical value or use the slider bar to rotate the flaw.

The completed rotation operation will be listed in this window.

A rotate operation can be undone by selecting the operation and clicking on **Undo**.



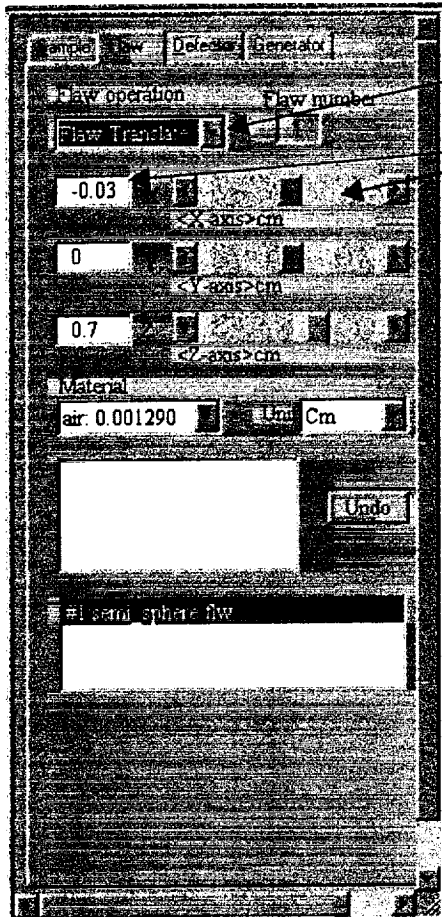
POSITIONING THE FLAW



The flaw in the right image has been rotated 25 degrees.

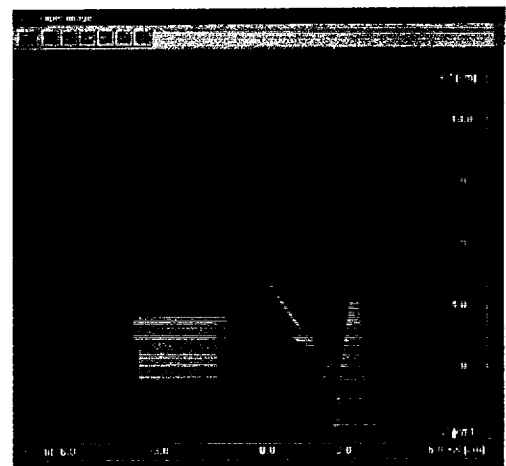
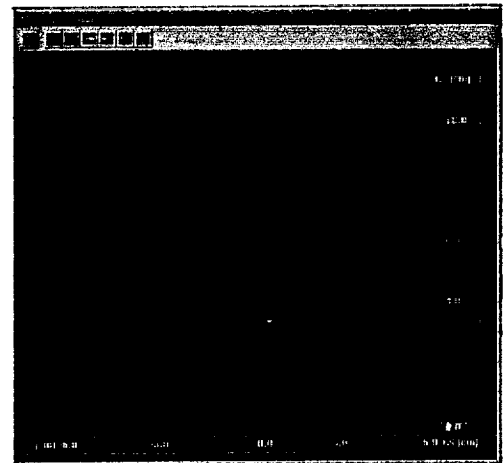
Once the flaw has been sized, it can be positioned and orientated in the part. In some cases, it may be necessary to switch back and forth between positioning and rotating the flaw to achieve proper placement.

1. Select the **Flaw Translate** option in the **Flaw Operation** dialog box in the flaw set-up window.
2. The flaw can be moved in any of three ways. First, it can be moved by clicking and dragging it in any of the view windows. The flaw will not track as fast as the mouse so stop occasionally to let the flaw catch-up with the mouse pointer. The flaw can also be moved typing a number in the position display box (the change takes effect when the enter key is depressed) or by using the slider bar or arrows.



Select **Flaw Translate** in the **Flaw Operation** dialog box

Type a numerical value in the entry box or use the slider bar to move the flaw to the desired location.



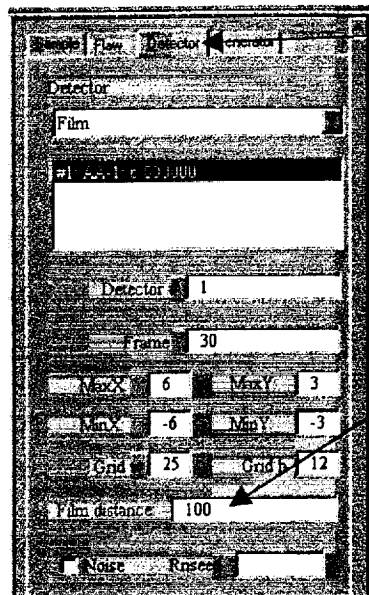
The flaw in the upper image has been moved down into the sample in the lower image. The sample in the lower image is displayed in the transparent mode so the flaw is visible.

SETTING THE SOURCE TO FILM DISTANCE

Once the sample is configured as desired in the x-ray vault, the distance of the source to the film should be set.

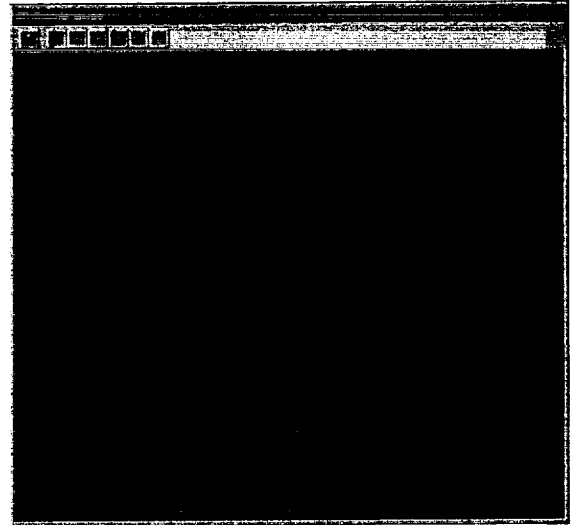
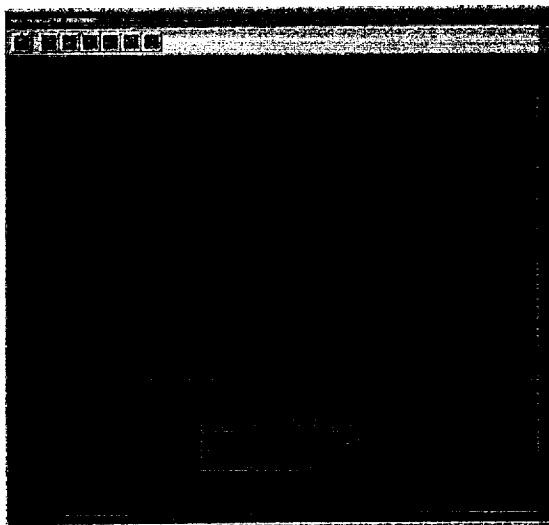
1. Select the **Detector** tab to display the detector set-up window.

2. In the **Detector** dialog box select the desired detector.
3. Set the source-to-film distance by typing in a value in the **Film distance** dialog box and press the enter key. The default value is 100 cm.



Select the **Detector** tab

Enter the desired source-to-film distance (in cm) in the **Film distance** box and press the enter key.



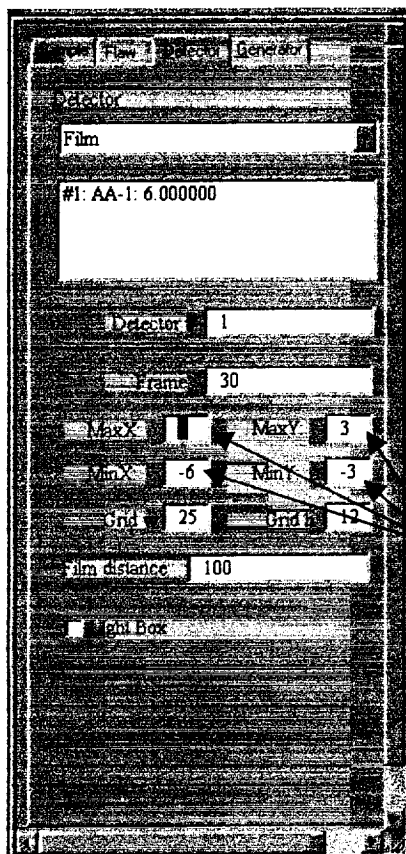
The Film to source distance in the left image is 100 cm and it has been changed to 50 cm in the right image. Note that the x-ray tube has moved closer to the film and the cone beam projection is smaller

SIZING AND POSITIONING THE FILM

Once the part has been placed in its desired position between the x-ray tube and the film, the film may need to be resized and repositioned to image the area of interest.

1. Select the top view (down arrow above the x-ray tube) for a view looking down from the x-ray tube. You will notice two things: the film (in red) is not entirely under the part and the cone of the x-ray beam (in pink).

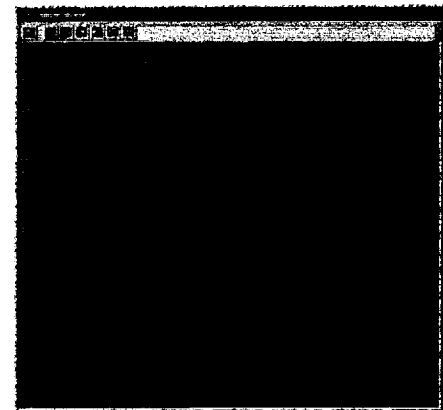
2. The film can be resized by clicking on the corner of the film and drag the corner to change the size and shape of the film. The film and also be resized by typing numerical values in the **MaxX**, **MinX**, **MaxY**, and **MinY** boxes on the **Generator** set-up window.
3. The film can be moved without changing its size by clicking on it away from the corners and dragging it to the desired location.
4. Now click on the second arrow above the xray tube and you will see a side view. The line represents the film plane. You will need to click and drag the part until it is even or slightly above the film plane. Looking at the left window you will see the numbers for your X, Y, Z positions have changed. **NOTE: when moving the part or film give the system time to keep up as the system will continue moving after you stop the mouse.** Return to the top view to confirm you have not moved the part off the film.



Clicking on the corner of the film and dragging as shown by the arrows in top right figure will change size and position of film to that shown in the bottom figure.



The film size and position can also be changed by entering numerical values. The values reflect the film edge distance from the center of the x-ray beam.



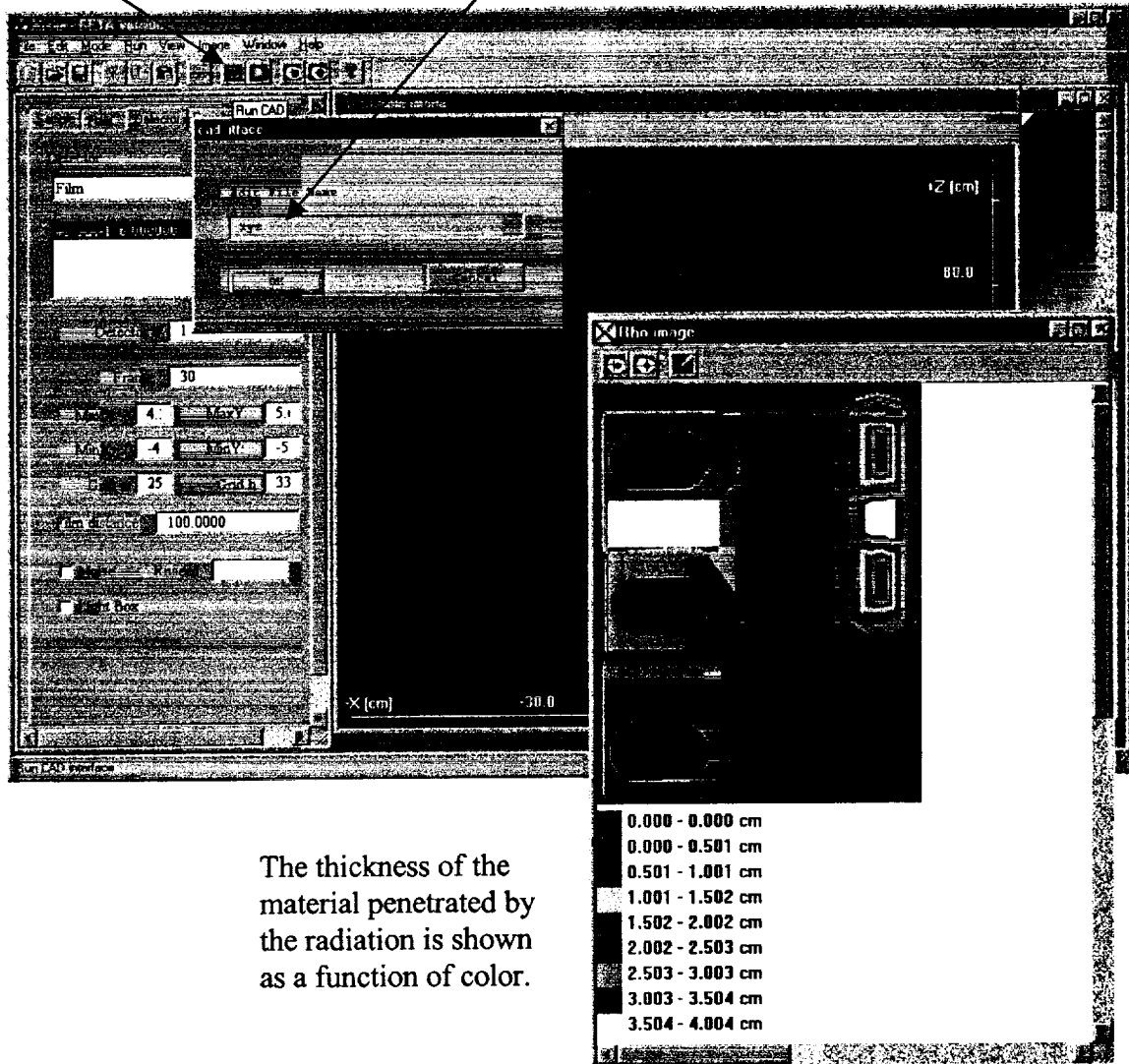
GENERATE THE 2D THICKNESS MAP FROM THE CAD FILE

Once the sample, the x-ray tube and the detector have been configured inside the vault, a 2D thickness map must be generated of the part from the CAD file. This step determines the amount of material that the x-rays must travel through based on the configuration of the sample and the flaw. This thickness map is calculated over the size of the detector so this operation must be completed after the part, source, and film are set. If any changes are made to the set-up, the 2D mapping step must be repeated.

1. Run the CAD 2D thickness mapping procedure by clicking the **Run Cad** hot button or by selecting **Cad** in the **Run** menu.
2. Edit the file name in the pop-up box to save the 2D thickness map. If the file name is not changed, the file will be overwritten the next time this procedure is preformed.
3. The 2D image of the part showing thickness of the material that the x-ray beam will travel though will be displayed.

Click the **Cad Run** hot button.

Enter a new file name (if desired) and click **OK**

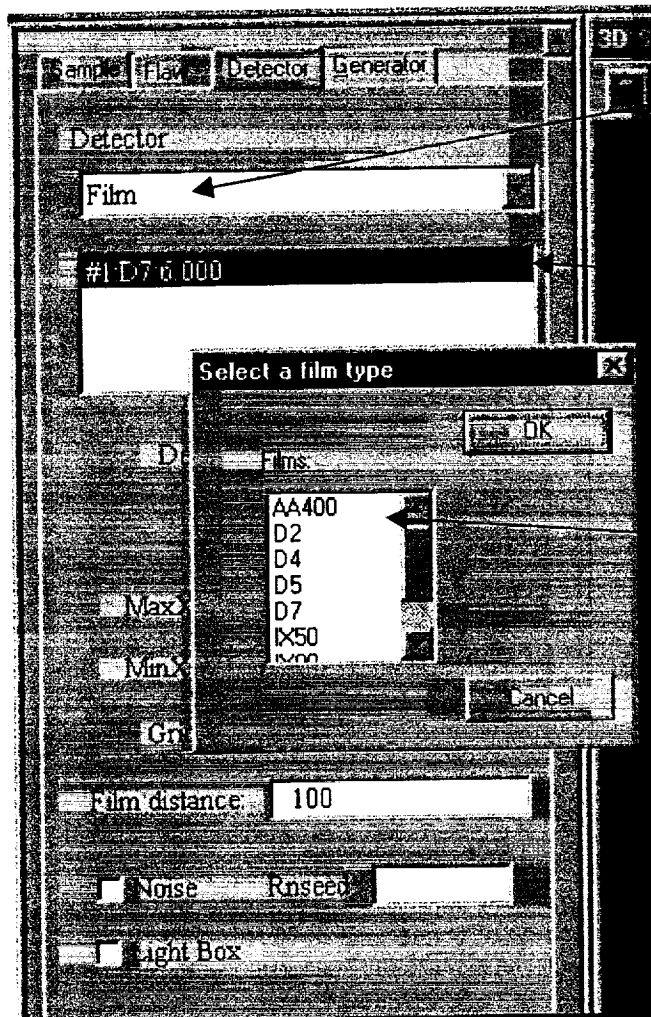


The thickness of the material penetrated by the radiation is shown as a function of color.

SELECTING THE FILM TYPE

A number of different films have been modeled in the XRSIM program. More information on the films included in the program is provided in Appendix B. It might seem that selecting the film should have been done when the film was resized, but there is a reason this step is placed here. The reason being is that prior to this step, anytime change in a parameter requires that the 2D thickness mapping process be run. Operations from this point on (changing the film type and adjusting the x-ray generator setting) do not require a new 2D thickness map to be generated.

1. Make sure film is selected in the **Detector** dialog box on the **Detector** set-up window (future releases of the program will have the capability to model an inspection using and image intensifier and to model double loads of film. These features are not currently available.)
2. Select a new film type by clicking on the film type in the second dialog box on the window. This action will open a film selection window.
3. A new film type can be selected by highlighting the desired film in the list of film in the **Films** dialog box and click the **OK** button.



On the Detector set-up window, make sure that Film is selected in the Detector dialog box.

A film type will be show in this box. To change the film type, click on the shown film and a film selection window will opened.

Highlight a new film type and click on the OK button.

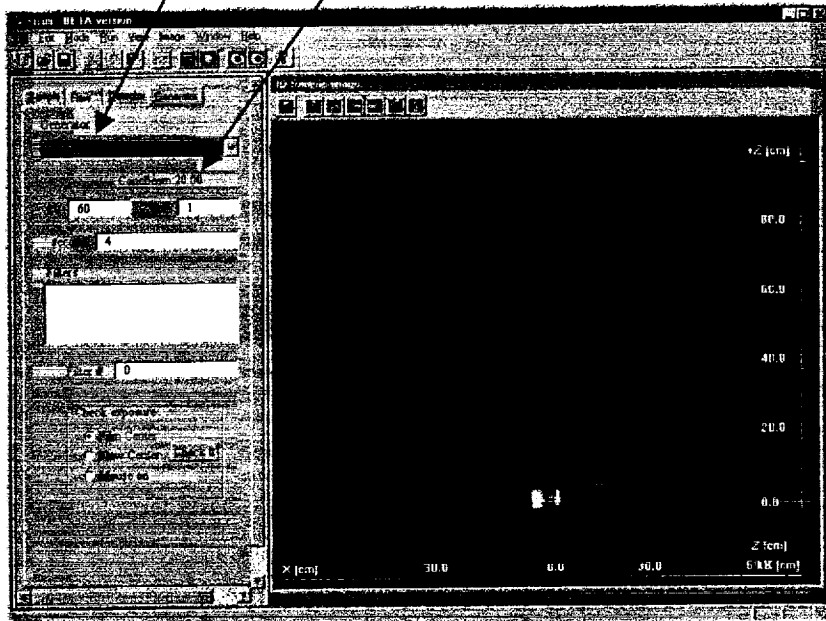
SELECTING AN X-RAY GENERATOR

Once the film type has been selected, a generator must be selected and the generator setting adjusted. A number of x-ray generator systems have been characterized and are modeled in XRSIM. More information on these systems is provided in Appendix C.

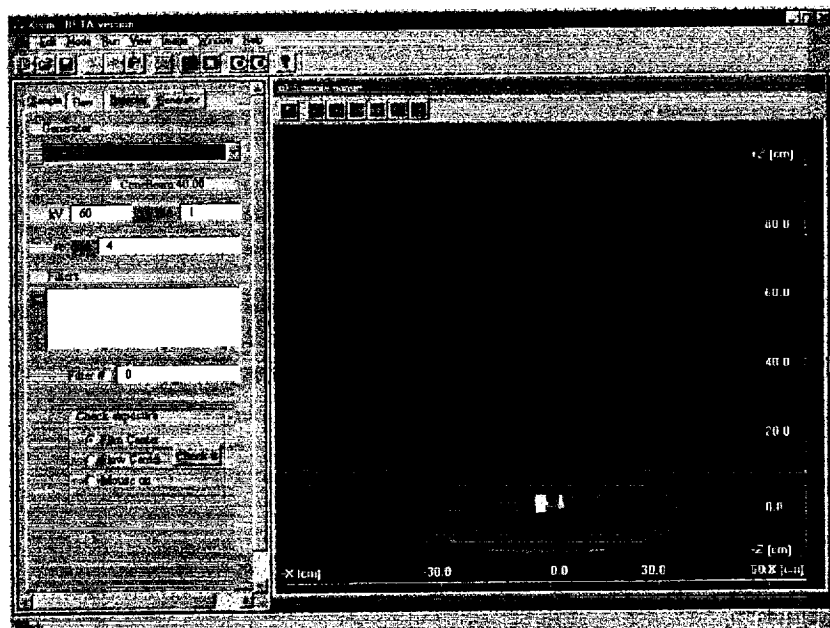
1. Display the generator set-up window by clicking on the **Generator** tab.

2. Select the desired generator from the list provided in the **Generator** dialog box. You will notice that the x-ray cone beam is different for some of the generators. The angle of the x-ray tube's cone beam is displayed in the set-up window and shown in the 3D window.

Select a generator from the list provided in the **Generator** dialog box
The angle of the cone beam for the tube is shown



In the upper image, the tube has a 20 degree cone beam while the tube in the lower image has a 40 degree cone beam

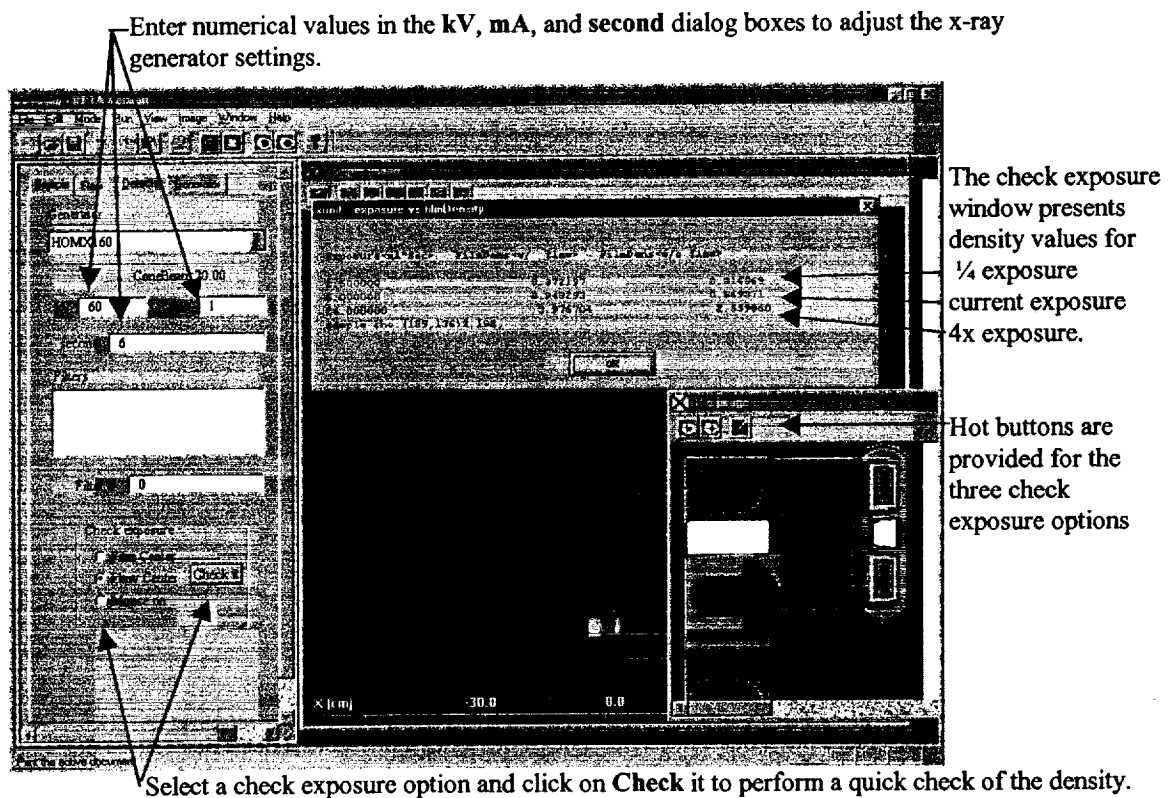


ADJUSTING THE X-RAY GENERATOR SETTINGS AND CHECKING THE EXPOSURE

Like any x-ray generator system, there are three generator variables in XRSIM that must be set to achieve the desired radiographic image. These variables include the voltage, which controls the energy of the radiation; the amperage, which controls the amount of radiation produced in a set time; and the timer, which controls the length of time that the film is exposed to the radiation. Once the variables have been adjusted, a quick check of the film density can be made to determine

if the exposure is correct. The density can be checked at the file center, at the flaw center (if a flaw has been included in the set-up), or at any point on the 2D thickness map.

1. Adjust the voltage (kV), amperage (mA), and exposure time (seconds) by typing a numerical value in the proper dialog box on the generator set-up window. **The enter-key must be pressed after a value is entered in order for the new value to take effect.**
2. Check one of the **Check exposure** options in the lower portion of **Generator set-up** window. A window will open and display the density values. The center row contains the densities for the current generator settings. The first row indicates what the densities would be if the exposure was decreased by a factor of four. The third row indicates what the densities would be if the exposure was increased by a factor of four. The exposure time is reported in mA-seconds since it is the product of these two variables that controls the exposure. When there is a flaw placed in the sample and the **Flaw Center** location is selected, the second column is the density at the center of the flaw and the third column is the density adjacent to the flaw. When the **Mouse On** location is selected, the density is displayed for any location where the mouse is clicked on the 2D-thickness map image. Hot buttons are also provided on the 2D-thickness map window for the three density check options.
3. Close the **Density Check** window by clicking on the **OK** button.

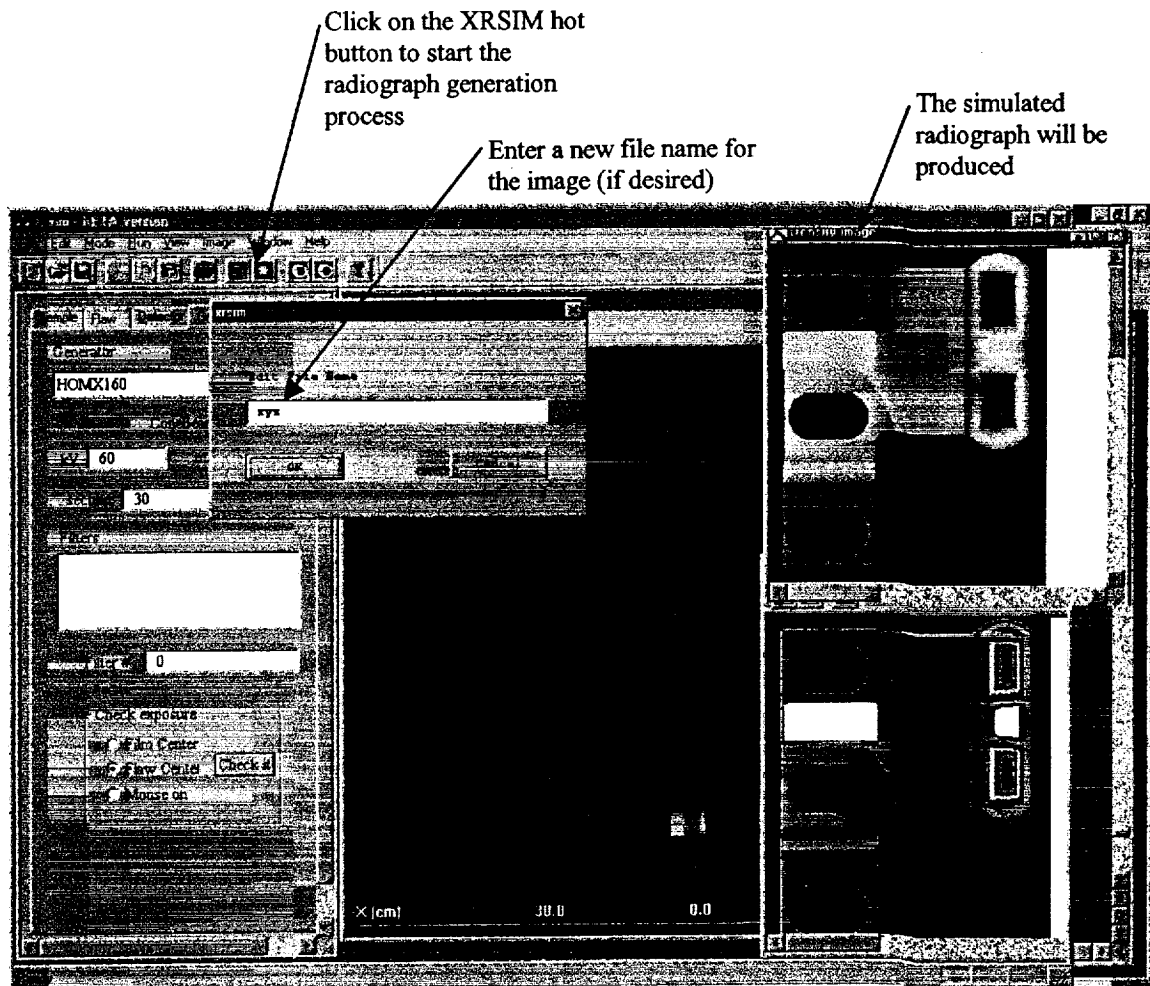


EXPOSING THE FILM TO PRODUCE THE SIMULATED RADIOGRAPH

Once the x-ray generator has been configured to yield the desired density, the simulated radiographic image can be produced. The film type and the x-ray generator setting can be changed and additional images can be quickly produced by repeating the procedure on this page. A new

2D-thickness map does not need to be generated unless the size, position, or orientation of the sample, flaw, or film is modified.

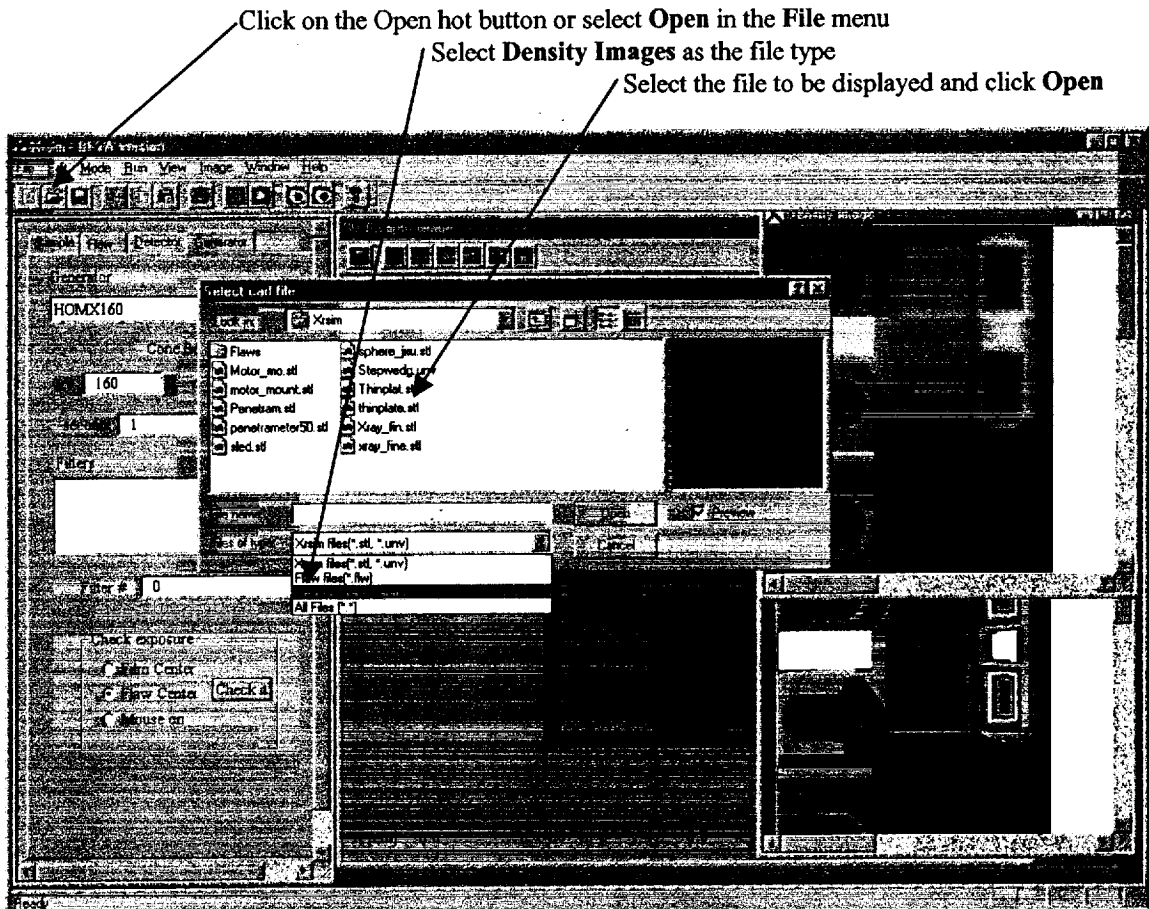
1. Run the process to produce the radiographic image by clicking on the **Run XRSIM** hot button or selecting **XRS** in the **Run** menu.
2. Edit the file name in the pop-up box to save the radiographic image and click on the **OK** button. The file will be automatically given an "xbm" extension. If the file name is not changed, the file will be overwritten the next time this procedure is preformed.



OPENING MULTIPLE RADIOGRAPHIC IMAGES

Multiple radiographic images can be open at the same time so that side-by-side comparisons of results can be made.

1. Click on the **Open** hot button or select **Open** in the **File** menu and the **File Open** window will appear.
2. Select **Density Images (*.xbm)** in the Files of type dialog box to display image files available to choose from.
3. Select a file to display and click the **Open** button. The image will be displayed.
4. Repeat the procedure to open additional images



ANALYZING THE IMAGE DENSITY USING THE SLICE FEATURE

XRSIM has an image analysis feature that can be used to obtain quantitative density information from the radiographic image. This feature produces a plot of density versus position for any horizontal or vertical line across an image. The density at the point where the cursor arrow is positioned is provided in the digital readout.

1. Open one or more of the density images to be analyzed.
2. Select the **Image** pull-down menu, then **Analysis**, then **Slice**. The **Slice** analysis window will be displayed.
3. Click the **Horizontal** button in the slice window if a plot of densities along a horizontal line across the image is desired; or click on the **Vertical** button if a plot of densities along a vertical line across the image is desired.
4. Click and hold down the left mouse button on the image to be analyzed. A horizontal or vertical line, depending on the selection in step 3, will be displayed across the image. The densities along this line will be plotted in the **Slice** window. A small "x" will indicate the position of the cursor arrow in the image and the density and pixel location for this point will be provided.
5. Click on **Done** in the **Slice** window to close the window

The screenshot shows a software interface with two main windows. On the left, there are two density images of a mechanical part. On the right, a 'Slice' window displays a line plot of density values. The plot has a y-axis from 0.0 to 6.0 and an x-axis from 0 to 500. A vertical slice line is drawn across the image, and a cursor arrow points to a specific pixel on this line. A small 'x' marks this pixel's location on the plot. A data box in the top right of the plot window displays the following information:

x[ptd]=183
y[ptd]=153
x[psd]=-5.84
y[psd]=-5.28
RealDns=4.87
Intensity=82

Annotations with arrows point to various parts of the interface:

- Open one or more density image files and position as desired on the screen.
- Select **Image**, **Analysis**, and **Slice** to open the **Slice** window
- Click and hold the mouse button down on the image to produce a slice line. The pixel density and location for the point that the cursor arrow points to is displayed in the slice window
- Click either **Horizontal** or **Vertical** to choose a slice direction (Horizontal was selected)
- The density and position of the pixel at the tip of the cursor arrow is displayed.
- The location on the plot is marked by a small "x."
- Click on **Done** to close the window